Mechanisms of efflorescence of alkali-activated slag

Liu, Chen; Li, Zhenming; Ye, Guang

DOI
10.1016/j.cemconcomp.2024.105811

Publication date
2024

Document Version
Final published version

Published in
Cement and Concrete Composites

Cement and Concrete Composites 155 (2025) 105811

Contents lists available at ScienceDirect

Cement and Concrete Composites

journal homepage: www.elsevier.com/locate/cemconcomp

Mechanisms of efflorescence of alkali-activated slag

Chen Liu [a], Zhenming Li [b,c,*], Guang Ye [a,**]

[a] Department of Materials and Environment (Microlab), Faculty of Civil Engineering and Geoscience, Delft University of Technology, 2628 CN, Delft, Netherlands
[b] School of Civil and Environmental Engineering, Harbin Institute of Technology, 518055, Shenzhen, China
[c] Guangdong Provincial Key Laboratory of Intelligent and Resilient Structures for Civil Engineering, Harbin Institute of Technology, 518055, Shenzhen, China

ARTICLE INFO

Keywords:
Efflorescence
Alkali-activated slag
Leaching
Cracking
Carbonation

ABSTRACT

Efflorescence presents not only as a cosmetic concern but also as a structural issue, which impacts the performance of alkali-activated materials (AAMs). In this study, the mechanisms of efflorescence of alkali-activated slag (AAS) pastes are investigated. First, the efflorescence of AAS pastes with different alkali dosages (3 %, 5 % and 7 %), activator types (sodium hydroxide (NH) and sodium silicate (NS)), exposure atmospheres (ambient, N_2 and 0.2 vol% CO_2), and relative humidities (40 %, 60 % and 80 %) was observed. Subsequently, leaching tests were performed and the impacts of efflorescence on AAS pastes at different heights were studied. It was found that a lower relative humidity facilitated more rapid and severe efflorescence. The positioning of efflorescence products was dependent on the porosity of the matrix. Compared to NH pastes, NS pastes subjected to semi-contact water conditions were more vulnerable to cracking problems, which turned out to be exacerbated by the formation of efflorescence products. A new method to quantify efflorescence was developed and it corresponded well with both efflorescence observations and leaching experiments. Furthermore, a competitive reaction between Ca and Na in the presence of carbonate ions was identified. $CaCO_3$, a representative product of natural carbonation, was rarely found in the regions where efflorescence products (sodium carbonate) formed. Regarding compressive strength, NS pastes were more adversely affected by efflorescence than NH pastes.

1. Introduction

Efflorescence refers to the formation of fluffy white deposits on the surface of materials, such as brick, concrete and stone [1,2]. In Portland cement (PC) systems, the main component of efflorescence products is calcium carbonate, which is generated through the reaction between soluble calcium and CO_2 (or CO_3^{2-}) in the water film on the surface of materials. These whitish deposits are loose and fluffy, presenting an aesthetic concern, but are generally considered harmless [3]. However, efflorescence in alkali-activated materials (AAMs) is more severe than in PC materials [4]. Due to the relatively lower content of Ca and higher alkalinity in AAMs, most Ca is incorporated into C-(N-)A-S-H gels instead of remaining in the pore solution. This results in the absence of calcium carbonate in efflorescence products. Conversely, considerable amounts of Na ions show high mobility in the pore solution, which leads to the formation of sodium (bi)carbonates with different amounts of chemically bound water. These sodium (bi)carbonates are the predominant efflorescence product in AAMs. Furthermore, the excessive formation of efflorescence products has the potential to induce substantial expansion, which can be detrimental to the structure of AAMs (especially geopolymers) if the resultant stress exceeds the strength of materials [6].

Historically, many studies have been carried out to investigate the efflorescence of AAMs. Recognizing the complexity of scenarios under which efflorescence occurs, people initially focused on developing strategies for efflorescence formation in earlier years. As outlined in [3], a water film and a sufficient duration are the requisites to generate efflorescence. Delair et al. [7] stored samples in a climate chamber at 100 % relative humidity for several days, followed by drying with a gradual decrease in relative humidity from 100 % to 50 %. They successfully observed the efflorescence on the metakaolin blended cement pastes by this method and found that the substitution of cement by metakaolin can reduce efflorescence. In another approach, Kani et al. [8] immersed samples in distilled water and exposed them together to open air at ambient temperature until the water was completely evaporated. They observed efflorescence on natural pozzolan blended geopolymers and found that calcium aluminate cements were effective in efflorescence reduction. Despite the visibility of efflorescence in the

* Corresponding author. School of Civil and Environmental Engineering, Harbin Institute of Technology, 518055 Shenzhen, China.
** Corresponding author.
E-mail addresses: C.Liu-12@tudelft.nl (C. Liu), Zhenmingli@hit.edu.cn (Z. Li), G.Ye@tudelft.nl (G. Ye).

https://doi.org/10.1016/j.cemconcomp.2024.105811
Received 17 June 2024; Received in revised form 14 September 2024; Accepted 21 October 2024
Available online 23 October 2024

aforementioned two methods, it is important to note that efflorescence formation may not continually accumulate after the samples have fully dried. This limitation can hinder the investigation of efflorescence with prolonged time. To address this issue, Zhang et al. [9] introduced a method by immersing the bottom of the sample in contact with water. This approach ensured a continuous water supply from the bottom of the sample, which can effectively promote ion and water transport and thus the efflorescence formation compared to previous methods. By using this method, they found that a higher curing temperature and a higher activator modulus can alleviate the efflorescence of fly ash-based geopolymer. In addition, the substitution of slag was beneficial in decreasing the rate of efflorescence, but it showed limited effects on reducing efflorescence potential as indicated by leaching results.

Since then, an increasing number of researchers have adopted this method to explore the efflorescence mechanisms of AAMs, including subflorescence [10], influential factors [11] and some potential mitigation strategies [12–17]. Zhang et al. [10] found subflorescence of fly ash-based geopolymer, which cooccurred with efflorescence but beneath the surface of the material. They assumed subflorescence to be harmful to geopolymer materials considering the crystallization pressure induced by the formation of efflorescence products. Longhi et al. [11] investigated the efflorescence of metakaolin-based geopolymers and reported similar results to [9] that the inclusion of soluble Si in activators was conducive to the densification of the matrix, the reduction in the alkali leaching and efflorescence formation. Maghsoodloorad et al. [18] reported that the employment of potassium-based activators can significantly reduce the efflorescence of alkali-activated phosphorus slag pastes. This was probably due to a lower content of free K^+ ions than Na^+ ions in the pore solution at the same alkali dosage and a higher solubility of potassium carbonate than sodium carbonate. Additionally, some effective mitigating strategies for the efflorescence of AAMs were developed by the addition of some admixtures i.e., nano SiO_2 [12,13], zeolite [14], silane [15], calcium hydroxide [16], calcium stearate [17] and sodium aluminate activators [19].

Quantitative evaluation of efflorescence was also of great importance to better understand this issue. Visual observation was the most commonly employed method to directly assess the extent of efflorescence [8–10]. Image analysis was a semi-quantitative manner by calculating the fraction of the surface that was covered by efflorescence products [20–23]. However, these two methods had limitations in taking the density and thickness of efflorescence products into account. Moreover, indirect methods were also developed to quantify the efflorescence. As leaching was a critical process impacting the formation of efflorescence [3], the ion concentration of Na^+, CO_3^{2-}, HCO_3^- and OH^- in the leachate of piece and powder samples was used to evaluate the efflorescence potential of AAMs [9,24]. In addition, weighing the mass loss of samples after the scraping of white deposits was also used to indirectly reflect the extent of efflorescence [16]. However, this method seemingly overlooked the subflorescence occurring beneath the surface.

According to the existing literature, several research gaps can be summarized. Firstly, the efflorescence mechanisms of AAMs have not been fully clarified. On one hand, the environmental factors influencing the efflorescence of AAMs, such as relative humidity, have been rarely reported. On the other hand, the impact of efflorescence on the samples at different locations or heights remains unclear [9,25]. Secondly, there is a lack of research on the efflorescence of plain slag-based AAMs. Most studies focus on fly ash- or metakaolin-based materials [9,11,25], as they are considered more porous and vulnerable to efflorescence problems compared to AAS materials. The addition of slag is normally used as an effective admixture to mitigate the efflorescence of geopolymers [9,26]. However, significant efflorescence, accompanied by cracks, has been observed in alkali-activated phosphorus slag pastes [27]. The underlying cracking mechanisms and their relationship with efflorescence seem to be unknown. Despite a decreasing availability of slag, driven by a low carbon emission, it presents as the most predominant precursor applied so far in AAM constructions. Thirdly, a universally accepted method for the quantification of efflorescence is still lacking, which inhibits a precise assessment of this phenomenon. Moreover, carbonation, typically considered the reaction between Ca and CO_2, has emerged as a significant deterioration in AAMs. The impact of carbonation on the microstructure of AAMs remains controversial [28–32]. This phenomenon may happen concurrently with efflorescence under ambient conditions, whereas the relationship between carbonation and efflorescence is still unclear.

To address these issues, efflorescence experiments were conducted on cylindrical AAS pastes with their bottom in contact with water. First, the effects of alkalinities (Na_2O content of 3 %, 5 % and 7 % to slag) and alkali activators (NH and NS), exposure atmospheres (ambient, N_2 and 0.2 vol% CO_2) and relative humidities (40 %, 60 % and 80 %) on visual efflorescence of AAS pastes were investigated. Then, leaching tests of AAS pastes in different sizes under different conditions were examined. The Na amount in efflorescence products of AAS pastes was quantitatively determined using inductively coupled plasma-optical emission spectrometry (ICP-OES). The distributions of absolute amount and relative proportion of Na in AAS cylinders were calculated by leaching results, and the relationship between efflorescence and leaching was established. Subsequently, the phase assemblage of efflorescence products of NH and NS pastes under ambient conditions and the impacts of efflorescence on the phase assemblage, gel structure and pore structure of AAS cylinders at different heights were comprehensively studied by X-ray diffraction (XRD), thermogravimetric analysis (TGA), Fourier-transform infrared spectroscopy (FTIR), and mercury intrusion porosimetry (MIP). The compressive strengths of AAS pastes with and without efflorescence were compared. Finally, the efflorescence process of AAS pastes was specified and the mechanisms of efflorescence of AAS pastes have been clarified. Hopefully, the insight of this work can contribute to a deeper understanding of efflorescence in AAS materials and facilitate the development of relevant standards and regulations regarding efflorescence.

2. Methodology

2.1. Materials and mixtures

Slag was used as the precursor for the preparation of AAS pastes. The chemical composition of slag was determined by X-ray fluorescence, as detailed in Table 1. The particle size distribution of slag ranged from 0.5 to 50 μm, with a median particle size of d_{50} of 18.2 μm. Four types of alkali activators were prepared by a commercial sodium hydroxide solution (50 wt%), a commercial sodium silicate solution (8.25 wt% Na_2O, 27.5 wt% SiO_2, and 64.25 wt% water) and deionized water.

The mix proportions of AAS pastes are shown in Table 2. To compare the impact of alkali activators on the efflorescence of AAS pastes, sodium hydroxide and sodium silicate were used, both with an alkali dosage of 5 % to the weight of slag, denoted as the "NH" and "NS" groups. To assess the effect of alkali dosage on the efflorescence of AAS pastes, NH pastes were prepared with alkali dosages of 3 %, 5 % and 7 %, referred to as "NH_3 %", "NH_5 %" and "NH_7 %", respectively. The water/slag ratio of four pastes was 0.43 and the silicate modulus (SiO_2/Na_2O) of the NS paste was 1.0.

The AAS pastes were prepared at room temperature (about 20 °C) with a Hobart mixer. The freshly prepared pastes were poured into polyethene cylindrical moulds (with dimensions of ϕ 35 mm × 70 mm) for efflorescence and leaching tests, and 4 cm × 4 cm × 16 cm prism moulds for compressive strength tests.

2.2. Efflorescence tests

AAS cylindrical samples were first sealed for 7 d and then cut in the shape of ϕ 35 mm × 50 mm. The cut surface of the cylinders was submerged in deionized water maintaining a depth of 10 (±1) mm in a glassy dish until 28 d. The environmental conditions for efflorescence

Table 1
Chemical composition of slag. (wt.%).

	CaO	Al_2O_3	SiO_2	MgO	Fe_2O_3	SO_3	K_2O	TiO_2	other	LOI
Slag	40.2	13.4	32.3	9.2	0.4	1.6	0.5	1.6	0.5	0.3

LOI = loss on ignition at 1000 °C.

Table 2
Mix proportions of AAS pastes.

AAS	Slag (g)	SiO_2 (mol)	Na_2O (mol)	Water (g)	Na_2O dosage (wt. %)
NH_3 %	1000	0	0.48	430	3 %
NH (NH_5 %)	1000	0	0.8	430	5 %
NH_7 %	1000	0	1.13	430	7 %
NS (NS_5 %)	1000	0.8	0.8	430	5 %

tests are shown in Fig. 1, including **(A)** ambient condition in a temperature and humidity-controlled room (air, T = 20 °C and RH = 55 %), **(B)** N_2 condition in a glove box (N_2, T = 20 °C and RH = 55 %, 1 atm), **(C)** CO_2 condition in a CO_2 chamber (0.2 % CO_2, T = 20 °C and RH = 55 %, 1 atm) and **(D)** different RH conditions in a tank with vents (air, T = 20 °C and RH = 40 %, 60 % and 80 %). The N_2 and CO_2 conditions were controlled by oversaturated $Mg(NO_3)_2$ solutions to maintain a RH of 55 %. The different RH conditions were controlled using oversaturated solutions of $MgCl_2$, $Mg(NO_3)_2$, and KCl, respectively. Vents located on the cover of tanks allowed the exchange of CO_2 with outside air. The RH under different conditions was monitored using an Extech® humidity/temperature data logger. The efflorescence of AAS cylinders was captured by a mobile phone for up to 28 d.

2.3. Leaching tests

Leaching tests of AAS pastes were carried out to establish the relationship between leaching and efflorescence and to quantitatively determine the efflorescence of AAS pastes. The ion concentration of Na in different leachates (Fig. 2) was measured using a PerkinElmer Optima 5300DV ICP-OES spectrometer. In Fig. 2A, a cylindrical sample (ϕ 35 mm × 50 mm, 80 ± 1 g) was first sealed for 7 d and then directly immersed in 150 ml of deionized water for 28 d. The leachate was referred to as "lea_cyl". In Fig. 2B, AAS pastes were first sealed for 7 d and then crushed into 2–4 mm pieces. 15 g of the pieces were submerged in 150 ml of deionized water for 28 d, with the resulting leachate labelled as "lea_pie". The above two leachates were used to determine the relationship between leaching and efflorescence.

Fig. 2C illustrates the efflorescence test of three 7 d AAS cylinders under ambient conditions. After 28 d of efflorescence, the solution in the

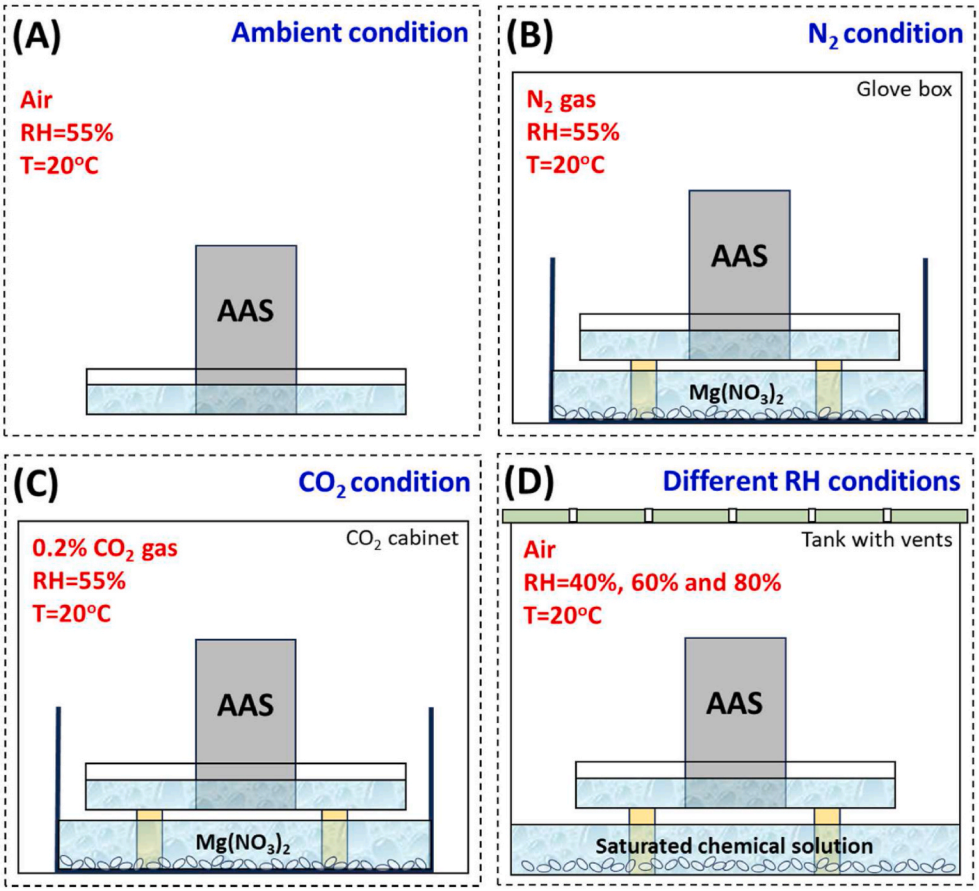

Fig. 1. Schematic diagram of the efflorescence tests for AAS cylindrical pastes exposed to different atmospheres. The samples were sealed for 7 d and then exposed to the above conditions for another 28 d. (A) ambient condition in a room (air, T = 20 °C and RH = 55 %), (B) N_2 condition in a glove box (N_2, T = 20 °C and RH = 55 %, 1 atm), (C) CO_2 condition in a CO_2 chamber (0.2 % CO_2, T = 20 °C and RH = 55 %, 1 atm) and (D) different RH conditions in a tank with vents (air, T = 20 °C and RH = 40 %, 60 % and 80 %).

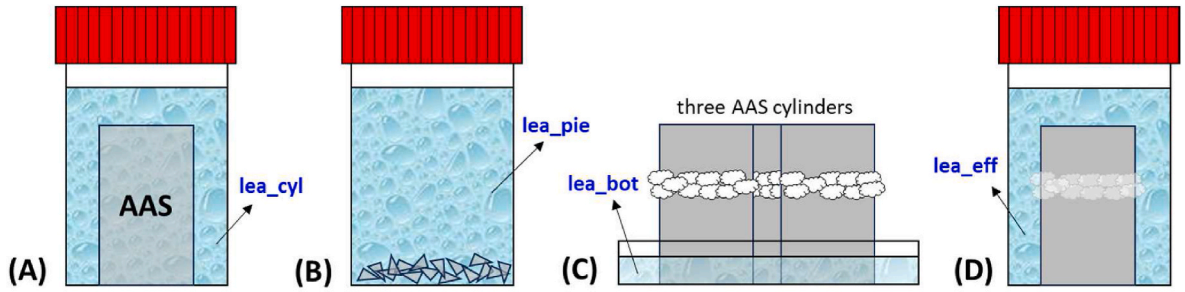

Fig. 2. Four types of leachates for the measurement of the ion concentration of Na in the leaching tests. (A) An AAS cylinder is immersed in 150 ml of deionized water for 28 d. The leachate is denoted as "lea_cyl". (B) 15 g of piece AAS pastes are immersed in 150 ml of deionized water for 28 d. The leachate is denoted as "lea_pie". (C) The bottom leachate of three AAS cylinders after 28 d of efflorescence under ambient conditions is referred to as "lea_bot". (D) The solution that dissolves the efflorescence products of three AAS cylinders is labelled as "lea_eff".

dish was collected and diluted to a total volume of 150 ml, which was denoted as "lea_bot". After the collection of the bottom solution, the three AAS cylinders attached by efflorescence products were immersed in the 150 ml of deionized water sequentially for ultrasonic cleaning, as shown in Fig. 2D. This process aimed to dissolve the efflorescence products on or beneath the surface of the cylinders. The resultant leachate was labelled as "lea_eff". It should be noted that the cleaning process lasted only 30 s to minimize the influence of excessive Na leached from AAS cylinders. The amount of Na in the efflorescence products can be calculated, which was considered a quantitative approach to evaluating efflorescence.

The Na concentration of four leachates was used to quantify the amount of leached Na from AAS pastes and the amount of Na in the efflorescence products. Then, we can use these values to further calculate the distribution of Na in a cylinder during the efflorescence process. Prior to this, the Na amount in the leachate per cylinder should be known. The calculation is shown as follows. Noted that ["lea_xxx"] refers to the Na concentration in the leachate of "lea_xxx".

Na amount in the leachate of "lea_cyl" per cylinder = ["lea_cyl"] × 0.15

Na amount in the leachate of "lea_pie" per cylinder = ["lea_pie"] × 0.15 ÷ 15 × 80

Na amount in the leachate of "lea_bot" per cylinder = ["lea_bot"] × 0.15 ÷ 3

Na amount in the leachate of "lea_eff" per cylinder = ["lea_eff"] × 0.15 ÷ 3

The Na amount in the leachate of "lea_pie", "lea_bot" and "lea_eff" per cylinder was used to calculate the distribution of Na. More specifically, the total amount of leachable Na in a cylinder was equal to the 'Na amount in the leachate of "lea_pie" per cylinder', assuming that all the free and weakly bound Na in the pore solution and gels can be leached away from the piece samples after 28 d of immersion. The Na amount distributed in the efflorescence products per cylinder was equal to the 'Na amount in the leachate of "lea_eff" per cylinder', while the amount of Na leached away from the bottom per cylinder was equal to the 'Na amount in the leachate of "lea_bot" per cylinder'. Finally, the distribution of the relative proportion of Na (wt. %) in a cylinder was calculated using the obtained distribution of the absolute amount of Na per cylinder.

2.4. Paste characterizations

The impacts of efflorescence on the property of AAS cylinders at different heights under ambient conditions (Fig. 1A) were investigated. Similarly, the samples were first sealed for 7 d and then exposed to ambient conditions for 28 d. Subsequently, the cylinders were ultrasonically cleaned (Fig. 2D) and evenly sliced into 4 thick sections, namely "bot", "low", "med", and "top", from the bottom upwards, as shown in Fig. 3. The exposed slices were immersed in isopropanol for 7 d to arrest the reaction of slag following the standard [33], and then dried in a vacuum oven at 20 °C until constant weight. Some of the slices were crushed into 4–6 mm pieces for MIP tests using a Micrometrics PoreSizer 9500. A high-pressure mercury intrusion process ranging from 0.17 to 210 Mpa, with a contact angle of 141°, enabling the pore size distribution ranging from 400 μm to 7 nm. The possible generation of the microcracks on samples during the high-pressure loading process was not considered. Some of the slices were crushed into pieces and then ground into powder for chemical characterizations, including XRD, TGA and FTIR. It is noted that the AAS pastes under sealed conditions were also characterized as the reference, namely "seal".

XRD test was conducted on a Bruker D8 Advance diffractometer with CuKα (1.54 Å) radiation. The detecting angles ranged from 5° to 70° with a step size of 0.02° and a swell time of 5s per step. TGA was performed using a NETZCH TG-449-F3-Jupiter instrument. Powdered samples (35 ± 1 mg) were heated from 40 °C to 1000 °C at a rate of 10 °C/min in an argon atmosphere. FTIR test was conducted on a Spectrum TM 100 Optical ATR-FTIR spectrometer. The tested wavenumbers started from 600 cm^{-1}–4000 cm^{-1} with a resolution of 4 cm^{-1}.

The compressive strength of AAS prisms was measured under three conditions: (1) ambient condition, (2) ambient condition with one side of the prism (4 cm × 16 cm) in contact with water at a depth of 10 mm, and (3) N_2 condition with one side of the prism in contact with water. The specimens sealed for 7 d and then exposed to the aforementioned three conditions for an additional 7 d (labelled "7 d") and 28 d (labelled "28 d") were measured. The measuring procedure was in accordance with NEN-196-1 [34]. The loading rate was 2.4 kN/s. Six replicates were used for each sample.

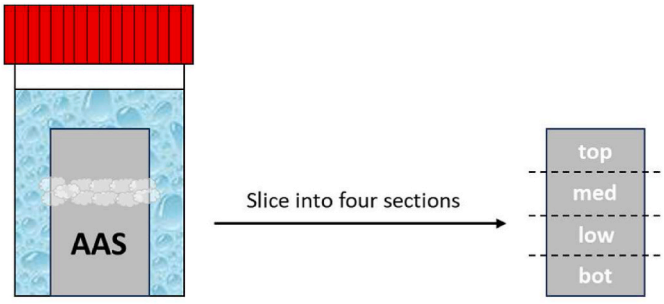

Fig. 3. Sample preparation before paste characterizations. The 7 d sealed cylinders after 28 d of efflorescence under ambient conditions are first ultrasonically cleaned, and then are sliced into four sections, designated "bot", "low", "med" and "top".

3. Results

3.1. Efflorescence observations of AAS pastes

3.1.1. Effect of alkali dosages

To investigate the impact of alkali dosages on the efflorescence of AAS pastes, NH cylinders with varying alkali dosages of 3 %, 5 % and 7 % were sealed for 7 d and then exposed to ambient conditions (Fig. 1A). As shown in Fig. 4, the NH_3 % group exhibits a lower severity of efflorescence compared to the NH_5 % and NH_7 % groups at both 7 d and 28 d, which indicates that the paste with a lower alkali content shows less efflorescence. This finding agrees with previous research [25,27,35], which is ascribed to a higher Na content in the cylinder of NH_7 %. Additionally, it is interesting to observe that the "efflorescence front" (the starting profile of white deposits from the bottom) of the NH_3 % cylinder is higher than that of the NH_5 % and NH_7 %. The height of the efflorescence front might be associated with the transport of water and ions in the cylinder. It is acknowledged that a decreased alkali dosage leads to a more porous and permeable pore structure of AAS materials [36,37], allowing an increased amount of water at the bottom to be absorbed upwards. This may result in a higher water penetration height in NH_3 % than in NH_5 % and NH_7 %. The percolated region shows high water contents (or RH), which are probably over the favourable range of RH for the formation of efflorescence products at a constant temperature. Therefore, the efflorescence front of NH_3 % is higher than NH_5 % and NH_7 %.

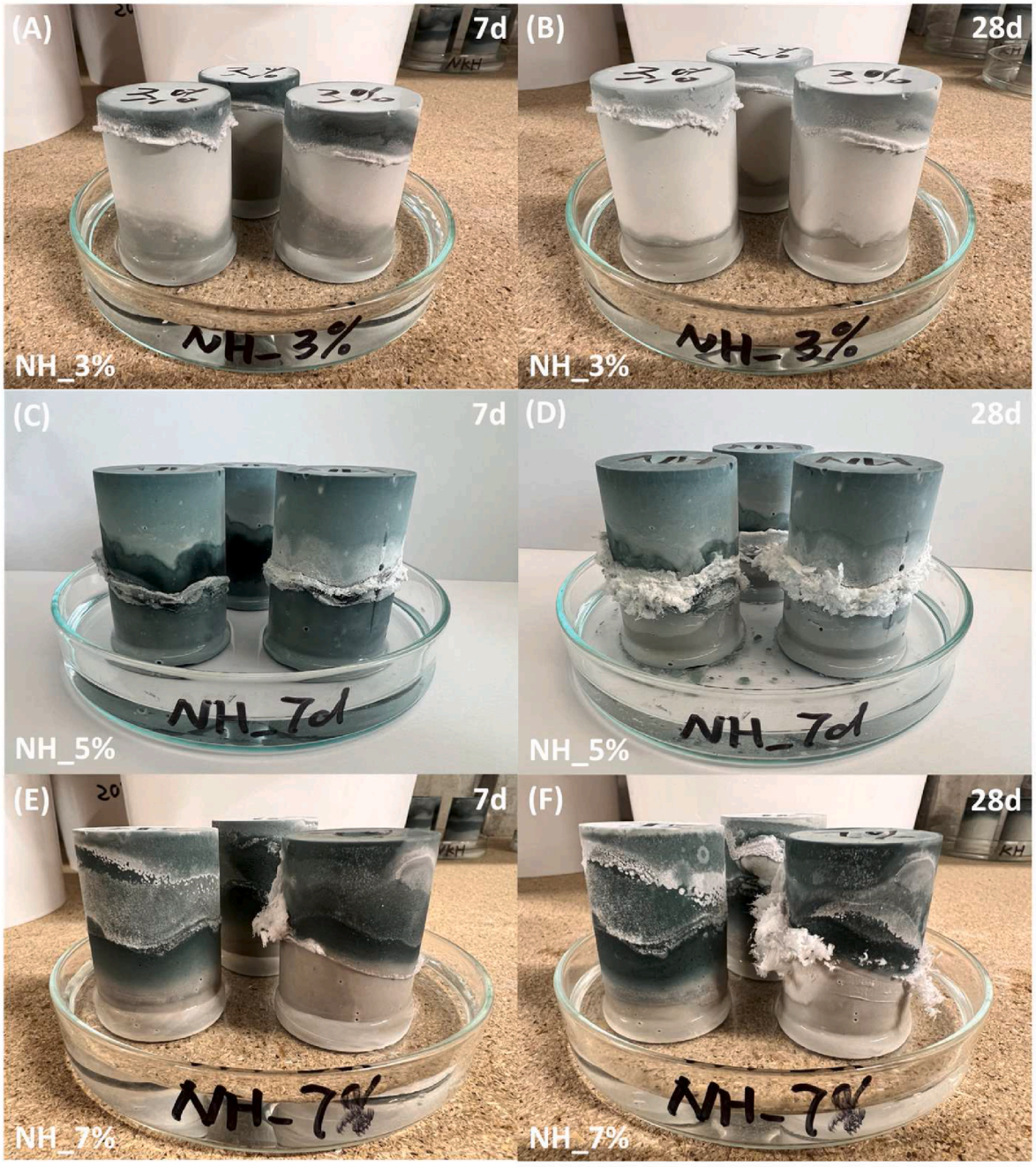

Fig. 4. Visual observation of efflorescence of NH cylinders with alkali dosages of 3 %, 5 % and 7 % exposed to ambient conditions for 7 and 28 d. The labels "NH_3 %", "NH_5 %" and "NH_7 %" indicate the NH paste with an alkali dosage of 3 %, 5 % and 7 %, respectively.

3.1.2. Effect of activator types

Fig. 5 shows the efflorescence of NH and NS cylinders under ambient conditions. The severity of efflorescence in both groups increases over time, with NH pastes exhibiting a more rapid development than NS pastes, as evident from photos captured after 1 d of exposure. These observations are consistent with an earlier work [9]. The presence of soluble silicate promotes the formation of gels, which is effective in reducing the porosity and pore connectivity of the matrix. A dense microstructure can impede the transport of water and Na, resulting in a lower efflorescence rate of NS samples.

In addition to the efflorescence rate, NH and NS cylinders also show distinct growth patterns of efflorescence products. As indicated in Fig. 5 at 3 d, white deposits on NH cylinders initiate from the second red line from the bottom, higher than that of NS cylinders beginning from the middle between the first and second red lines. In conjunction with the preceding observations illustrated in Fig. 4, the lower efflorescence front of the NS cylinder is due to a denser microstructure. Additionally, on NH samples, fluffy white deposits only progressively accumulate around the second red line, whereas those on NS samples can spread upwards until the top. Significant cracks are also observed at the top of NS cylinders. Similar observations regarding the efflorescence of alkali-activated phosphorus slag were also reported in [27]. Unlike the efflorescence of NH samples with different alkali dosages (Fig. 4), the severity of the efflorescence on NH and NS samples is hard to evaluate visually. The white deposits on NH samples are concentrated and thick, while those on NS samples are more widespread but thinner. Therefore, a quantitative manner for assessing the severity of efflorescence is highly necessary.

After 28 d of efflorescence, the samples were cleaned with an ultrasonic bath to remove the white deposits. The appearance of the side and top surfaces of AAS cylinders is presented in Fig. 6. As shown in Fig. 6A, discolouration is observed on both NH and NS cylinders. The middle section of the NH cylinders, as well as the entirety of the NS cylinder above the immersed portions, display a darker colour than the immersed sections. As reported in [38], the specific blue/green colouration observed in slag-based materials is attributed to the presence of trisulfur radical anion (S_3^-). These ions are vulnerable to oxidation under ambient conditions, resulting in surface discolouration. In the combination of Fig. 5, the blue/green regions in Fig. 6A are exactly the regions where efflorescence forms. So far, no research has claimed the underlying mechanisms behind this phenomenon. We tentatively consider that there is a competition between efflorescence formation and oxidation of trisulfur anions, and the latter reaction might be hindered by the former.

Moreover, it also can be seen that more significant cracks are observed on both the top and sides of the NS cylinders. In fact, large drying shrinkage of AAS materials has been extensively confirmed in early studies [39,40], which can lead to severe cracking problems under ambient conditions. In addition, the magnitude of dry shrinkage is dependent on the RH of exposure conditions, with a lower RH exhibiting more substantial shrinkage [41,42]. The scenario of the bottom of cylinders in contact with water can induce an uneven distribution of RH and thus an uncoordinated distribution of shrinkage, which in turn, significantly heightens the cracking potential of AAS cylinders. As reported in [27], similar cracks on the upper sides of the phosphorus slag activated by sodium silicate are also observed during efflorescence. They hypothesise this phenomenon to the growth of efflorescence products. To better understand this cracking issue, we conducted the efflorescence tests under N_2 conditions.

3.1.3. Effect of exposure atmospheres

N_2 atmospheres can eliminate the influence of CO_2 and efflorescence formation on AAS cylinders. As shown in Fig. 7, no efflorescence products but some cracks are observed on AAS cylinders under an N_2 atmosphere. Besides, the magnitude of cracks appears to be smaller than those under ambient conditions (Fig. 6). This indicates that the semi-immersed condition is the main reason triggering the cracking of NS cylinders, and the accumulation of efflorescence products along the cracks under ambient conditions can further exacerbate the cracking problems.

To understand the impact of CO_2 concentration on the efflorescence of AAS pastes, cylinders exposed to 0.2 % CO_2 atmosphere are also

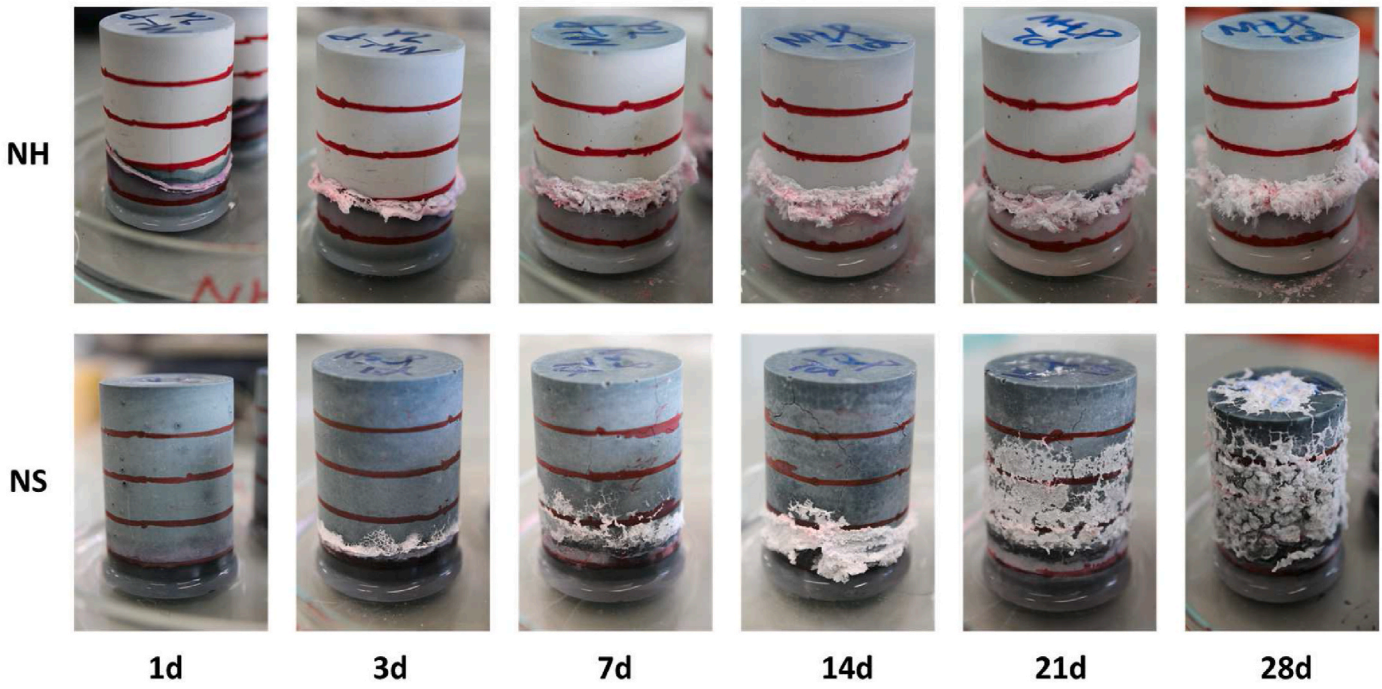

Fig. 5. Visual observation of efflorescence of NH and NS cylinders under ambient conditions with time. The cylindrical samples are marked by parallel red lines at 1 cm intervals to clearly show the location of efflorescence products. (For interpretation of the references to colour in this figure legend, the reader is referred to the Web version of this article.)

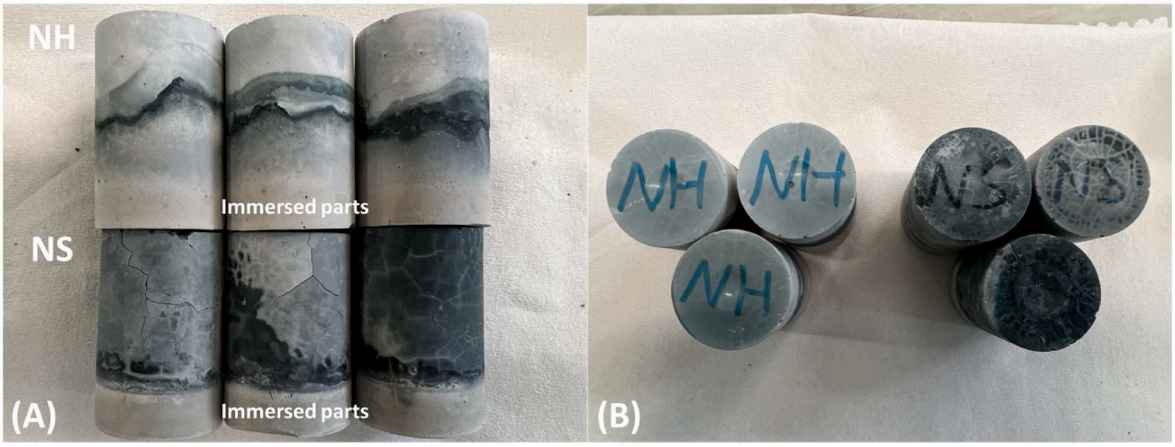

Fig. 6. (A) Side and (B) Top surfaces of ultrasonically cleaned NH and NS cylinders after 28 d of efflorescence under ambient conditions.

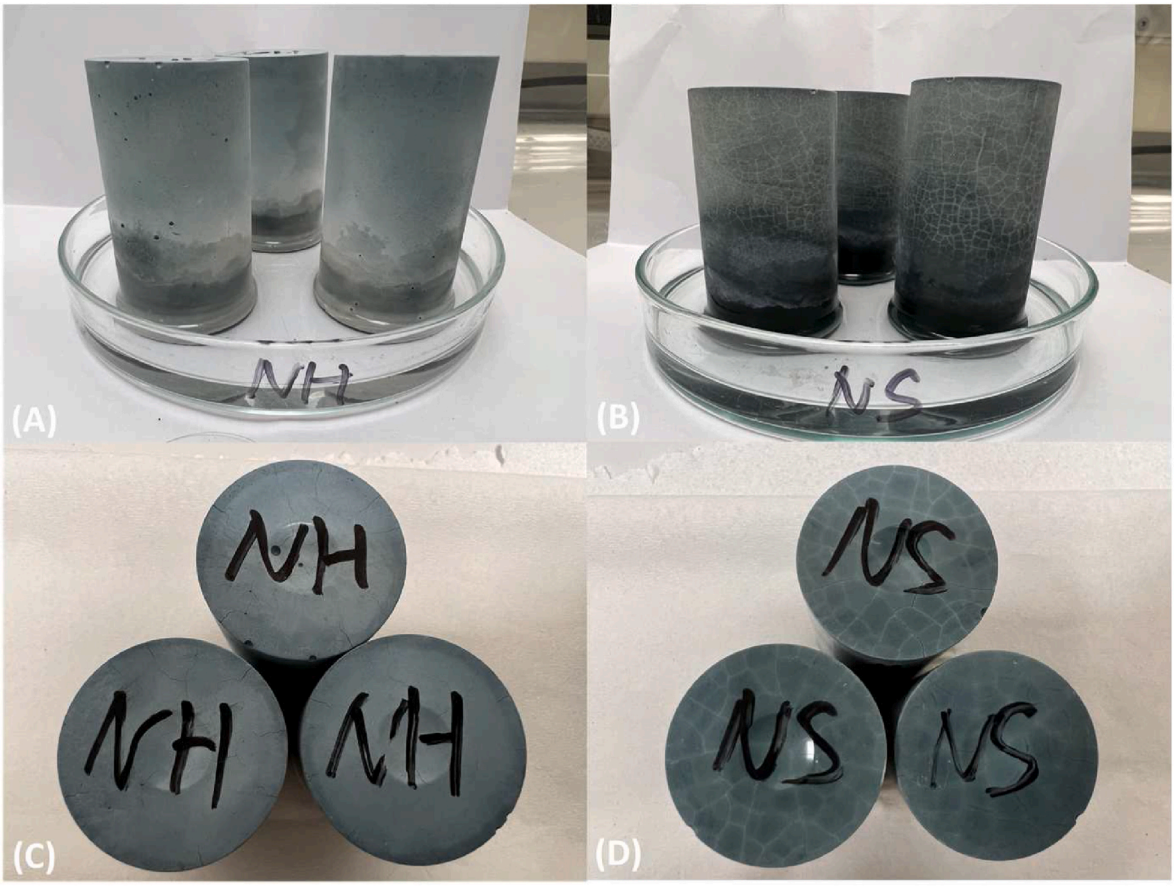

Fig. 7. (A) and (B): NH and NS cylinders exposed to under semi-contact water conditions. (C) and (D): Top surfaces of NH and NS cylinders after exposure to N_2 atmosphere for 28 d.

observed, as shown in Fig. 8. Consistent with the observations in Fig. 5, the efflorescence front of NH cylinders is higher than that of NS ones. However, the white deposits appear thicker and denser on both NH and NS cylinders under CO_2 conditions than ambient conditions. This indicates that an elevated CO_2 concentration promotes the formation of efflorescence products. Additionally, it can be seen that the white deposits on NS cylinders under CO_2 conditions tend to accumulate at low positions rather than developing towards the top as observed under ambient conditions (Fig. 5), while the cracks are also observed on NS cylinders. A possible reason for this phenomenon could be the internal circulation system in the CO_2 cabinet, which may provide a more significant drying process on the top of samples than under ambient conditions. The top sections of NS cylinders with cracks in the CO_2 chamber can be dried more quickly and intensively than under ambient conditions. However, efflorescence products fail to form under dry conditions. Therefore, the white deposits predominantly form at the low and medium parts of NS cylinders.

3.1.4. *Effect of relative humidities*

Fig. 9 displays the efflorescence of NH cylinders under different RH

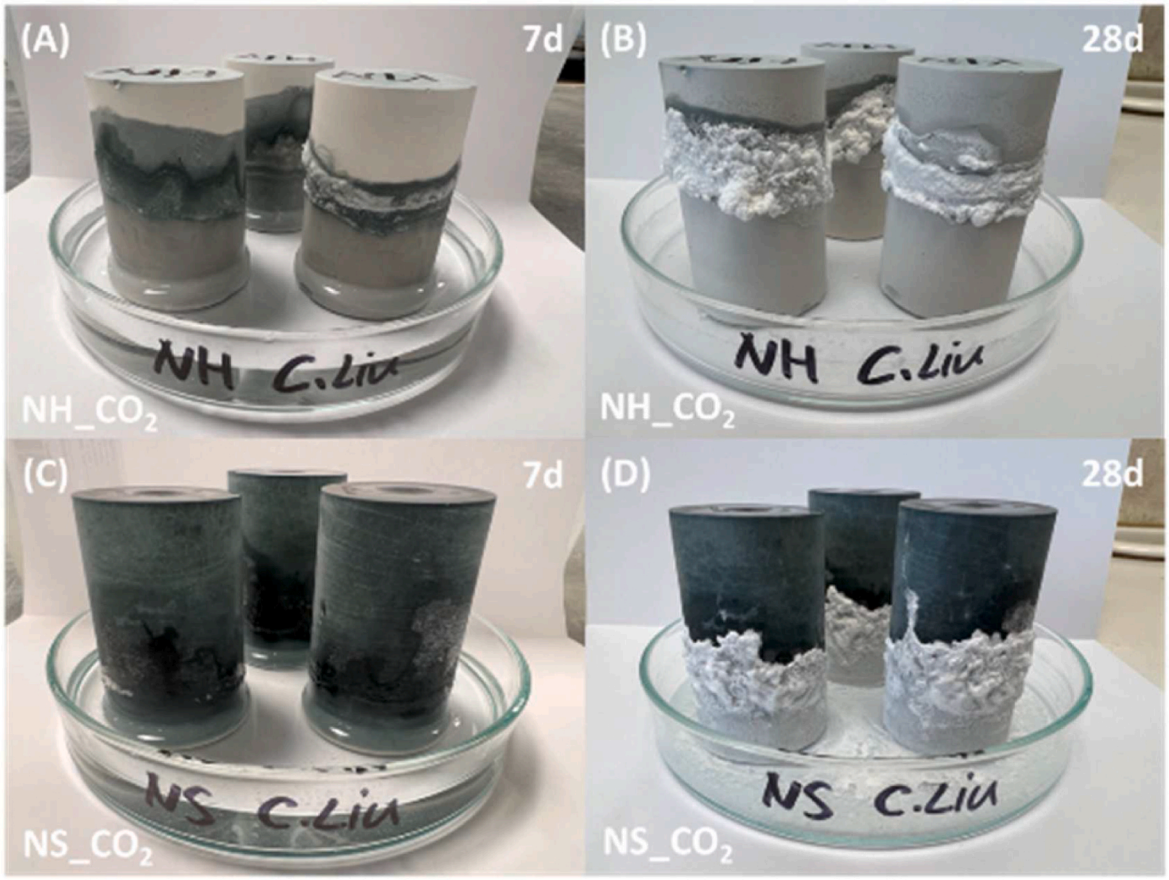

Fig. 8. Visual observation of efflorescence of NH and NS cylinders exposed to 0.2 % CO_2 conditions for 7 and 28 d. The labels "NH_CO_2" and "NS_CO_2" indicate the NH and NS pastes exposed to 0.2 % CO_2 conditions.

conditions. As observed in Fig. 9A–C, the NH cylinder under RH = 40 % has already shown efflorescence after 1 d of exposure, whereas those stored under RH of 60 % and 80 % do not. This indicates that the sample exposed to a lower RH environment undergoes a more rapid efflorescence process. With the extension of exposure time, white deposits gradually emerge and accumulate on cylinders under RH of 60 % and 80 %. During 28 d of exposure, the efflorescence on NH_40 % samples is constantly more intensive than that on NH_60 % and NH_80 % ones. In addition, some drops of liquid are discernible on NH_80 % samples (Fig. 9F and **I**). This implies that moisture under high RH environments may condense on the surface of cylinders, which results in a reduced formation of visible efflorescence. Therefore, it is evident that RH plays a significant role in both the rate and severity of efflorescence.

It should be noted that the white deposits on NH cylinders in Fig. 9 develop at both the medium and top sections of the cylinder, contrasting with the observation in Fig. 5. This distinction probably arises from the surrounding distribution of CO_2. Under ambient conditions (Fig. 1A), cylinders are exposed to fresh air, among which CO_2 is evenly and constantly distributed around the cylinders at different heights. However, under different RH conditions, fresh CO_2 is only supplied through the vents of the tank (Fig. 1D), potentially resulting in a higher concentration of CO_2 at the top of cylinders than at low positions. This uneven distribution of CO_2 contributes to a preferential formation of efflorescence products at the upper regions of cylinders.

3.2. Leaching tests of AAS pastes

3.2.1. Na amount in different leachates

Leaching is regarded as a proxy of efflorescence, which partly reflects the efflorescence potential of materials [9]. Fig. 10A shows the Na amount in four types of leachates per cylinder calculated by ICP results (section 2.3). The "lea_cyl" and "lea_pie" refer to the leachates of AAS pastes in cylinder and piece shapes, respectively. The Na amount in the leachate of "lea_pie" is significantly higher than that of "lea_cyl", attributed to the size effect of materials. Besides, the paste with a higher alkali dosage shows a higher leaching amount of Na, consistent with the above efflorescence observation (Fig. 4). Interestingly, the Na amount in the "lea_pie" of NS_5 % is slightly lower than that of NH_5 %, while the Na amount in the leachate of "lea_cyl" of NS_5 % is much higher than NH_5 % and even NH_7 %. Regarding the former result, it is due to the higher content of C-(N-)A-S-H gels in NS pastes than in NH pastes. These gels require more Na^+ ions to counterbalance the charge in the interlayer, resulting in a lower concentration of free Na^+ ions in the pore solution [43]. As for the latter result, the leaching of cylinders is a transport issue, closely correlated with surface microstructure. While a higher silicate modulus results in reduced porosity, the surface of the NS cylinder suffers from the cracking problem under immersed conditions, which is the main reason why the cylinder of NS_5 % exhibits a higher leaching amount of Na than NH_5 %.

The leachate of "lea_bot" refers to the solution in contact with the bottom of cylinders. It is shown in Fig. 10A that the leached Na amount increases with the increase in alkali dosages in NH pastes, and different types of pastes with the same alkali dosage show comparable leaching amounts of Na in the leachate of "lea_bot". This indicates that the leached amount of Na from the bottom of cylinders during efflorescence depends on the initial alkali contents. The Na amount in the leachate of "lea_eff" indicates the amount of Na in the efflorescence products (sodium (bi) carbonate), serving as a quantitative indicator for evaluating the severity of efflorescence of AAS cylinders. As can be expected, the NH_7 % paste shows a higher Na amount than NH_5 %, followed by the NH_3

Fig. 9. Visual observation of efflorescence of NH cylinders subjected to different RH conditions of 40 %, 60 % and 80 % for 1, 7, and 28 d. The labels "NH_40 %", "NH_60 %" and "NH_80 %" indicate the NH paste subjected to the RH of 40 %, 60 % and 80 % conditions at 20 °C, respectively.

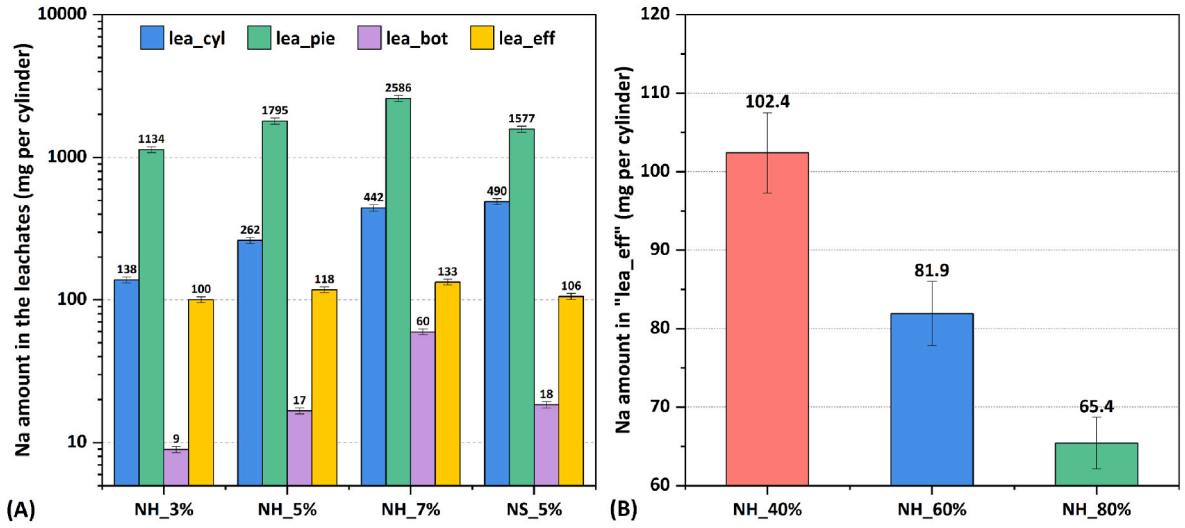

Fig. 10. (A) Na amount in different leachates of AAS pastes per cylinder. **(B)** Na amount in the leachate of "lea_eff" per NH cylinder under RH = 40 %, 60 % and 80 % conditions.

% paste, which aligns with the observations presented in Fig. 4. Moreover, the Na amount in the leachate of "lea_eff" per NH cylinder subjected to different RH conditions is shown in Fig. 10B. It is evident that the Na amount in the leachate of "lea_eff" increases with the decrease of RH, which matches the observation in Fig. 9. The feasibility of this quantitative method is validated again. It is also seen that the Na amounts in the leachate of "lea_eff" under different RH conditions are all lower than that of "NH_5 %" under ambient conditions. This is probably due to an insufficient CO_2 supply from the vents of the tank.

3.2.2. Na distribution in AAS cylinders during efflorescence

Fig. 11A shows the distribution of the absolute amount of Na in an AAS cylinder by mass. It is observed that the total leachable Na ("bottom-leached" + "efflorescence" + "remained") in NH cylinders increases with the increase of the alkali content. The remained amount of leachable Na in the paste with a higher alkali dosage is also higher than that with a lower alkali dosage. This part of Na can be regarded as the efflorescence potential, and it is recommended to utilize this method for predicting the efflorescence potential of AAS materials. Fig. 11B shows the distribution of the relative proportion of Na in AAS cylinders under ambient conditions. It can be seen that the majority of leachable Na (90.5–92.6 %) remains in the cylinder after 28 d of efflorescence. A minor fraction of Na (5.1–8.7 %) is present in the efflorescence products, while a minimal proportion of Na (0.8–2.3 %) leaches from the bottom. Compared with NH_5 % and NS_5 %, the fractions of "bottom-leached", "efflorescence" and "remained" Na are comparable. Even though the presence of Si can densify the microstructure, it appears that it fails to significantly hinder the leaching of Na. As for the three NH pastes, it is interesting to note that the proportion of Na in the "efflorescence" part decreases with an increase in alkali dosages, while the proportion of Na in the "bottom-leached" part increases with the increase in alkali dosages. In fact, the relative Na distribution can reflect the mobility of Na, with a higher proportion of Na indicating a higher mobility of Na. Therefore, the porosity contributes more than alkali dosages to impacting the mobility of Na in terms of efflorescence. Conversely, the alkali dosages have a greater influence on the mobility of Na concerning leaching than the porosity does. This indicates different main driving forces between leaching and efflorescence. The former is more related to the gradient of ion concentration, while the latter is more dependent on the transport of moisture and ions.

3.2.3. Relationship between leaching and efflorescence

Fig. 12 shows the relationship between the Na amount in the efflorescence products and the leachate of "lea_pie" and "lea_cyl". As shown in Fig. 12A, the Na amount in the leachate of AAS piece pastes shows a positively linear relationship with that in the leachate of efflorescence products. This suggests that the leaching of Na from piece pastes can reflect the severity of the efflorescence of AAS cylinders. However, the Na amount in the leachate of AAS cylinder samples does not show a perfect linear correlation with efflorescence. The Na amount in the leachate of "lea_cyl" of the NS_5 % cylinder is significantly higher than that of the NH_5 % cylinder, although both of the two pastes show the same alkali dosage. As mentioned above, this is mainly attributed to the cracking of NS cylinders when subjected to water immersion [43,44], which increases the permeability of the surface pastes and promotes the leaching of Na. Therefore, it is better to use the leaching result of piece samples to assess the efflorescence potential of AAS materials, which can minimize the size effect and cracking problems.

3.3. Characterizations of AAS pastes

In this section, the impact of efflorescence on the properties of NH and NS cylinders with an alkali dosage of 5 % under ambient conditions was investigated, representing two typical types of AAS materials. First, the component of efflorescence products of NH and NS cylinders was identified. Then, the phase assemblage, gel structure and pore structure of AAS cylinders at different heights after 28 d of efflorescence were examined. Finally, the compressive strength of AAS pastes with and without efflorescence was compared.

3.3.1. XRD

Fig. 13 shows the XRD pattern of the white deposits on NH and NS cylinders after 28 d of efflorescence under ambient conditions. In agreement with previous works [9,13,15,16,26,45,46], the primary

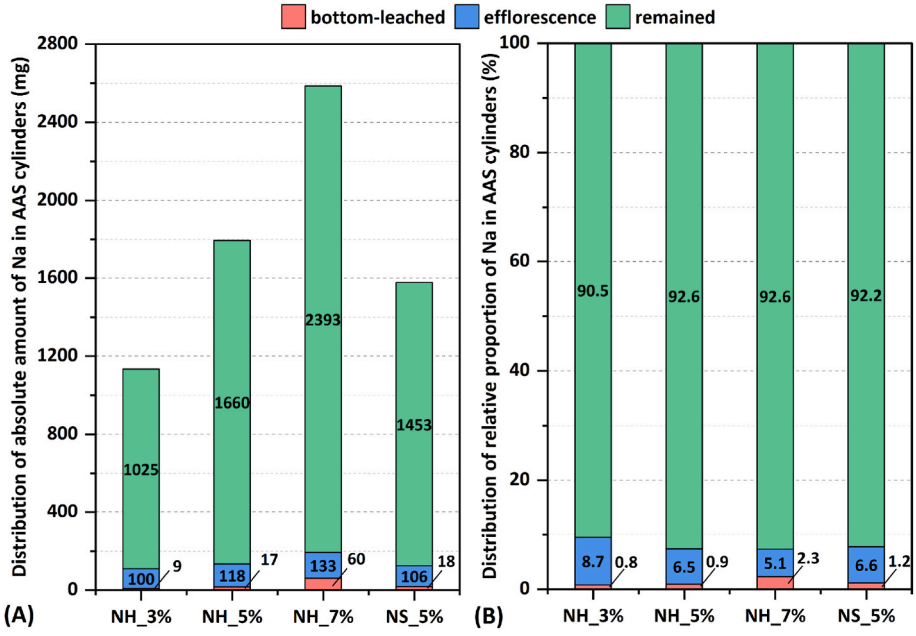

Fig. 11. (A) Distribution of the absolute amount of Na in AAS cylinders under ambient conditions. (B) Distribution of the relative proportion of Na in AAS cylinders under ambient conditions. "bottom-leached" indicates the Na leached away from the bottom of the cylinder during efflorescence tests. "efflorescence" denotes the Na in efflorescence products. "remained" refers to the Na remaining in the cylinder after efflorescence tests. The sum of "bottom-leached", "efflorescence" and "remained" Na is the total leachable Na in a cylinder.

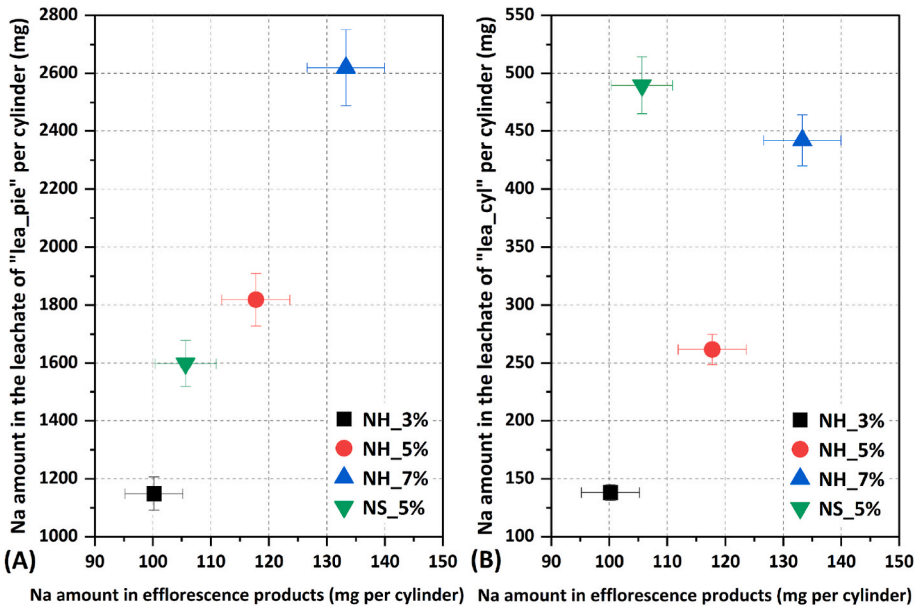

Fig. 12. Relationship between the Na amount in efflorescence products per cylinder and the Na amount in the leachate of (A) "lea_pie" and (B) "lea_cyl" per cylinder. The Na amount in efflorescence products is obtained from the leachate of "lea_eff".

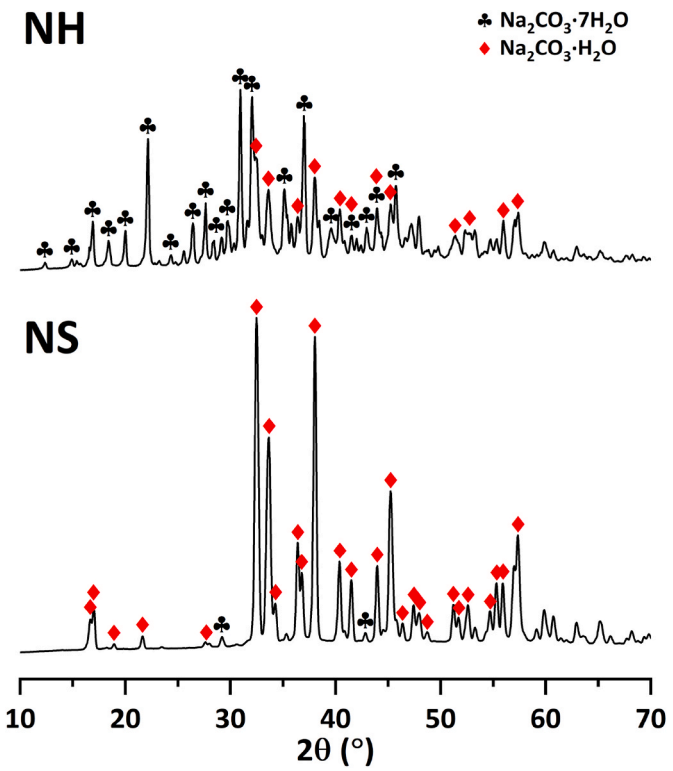

Fig. 13. XRD patterns of the efflorescence products on the NH and NS cylinders under ambient conditions for 28 d.

efflorescence product of both groups is identified as hydrated sodium carbonate. However, the efflorescence product of the NH pastes is dominated by $Na_2CO_3{\cdot}7H_2O$ whereas that of NS pastes is $Na_2CO_3{\cdot}H_2O$. This indicates a higher presence of chemically bound water in the white deposits of NH cylinders. As stated in [47], the chemically bound water of sodium carbonate is dependent on the humidity of its growth environments. As both types of pastes are exposed to the same ambient conditions (Fig. 1A), the distinction of chemically bound water in efflorescence products is mainly due to the water supply from the bottom of the cylinder. Specifically, the NH paste shows a more porous structure, allowing it to absorb more water from the bottom. A higher water content in the pore structure is therefore conducive to the increase of chemically bound water in efflorescence products.

Fig. 14A shows the XRD pattern of 7 d NH pastes subjected to 28 d of efflorescence under ambient conditions and 28 d of sealed conditions, respectively. In general, C-(N-)A-S-H gels [48] and hydrotalcite-like phases [49] are the two main phases dominated in NH pastes under sealed conditions, while calcite and vaterite, two $CaCO_3$ polymorphs [50], are the CO_2-bearing phase detected in the sample under ambient conditions. This is consistence with the results in [29,51], in which vaterite is the main carbonation product of AAS pastes subjected to accelerated carbonation. The content of vaterite increases with the increase of curing time and CO_2 concentration. Besides, as shown in Fig. 14A, the phase assemblage of the pastes exhibits slight differences at different heights of cylinders. For instance, while the "top", "med", "low" and "bot" pastes are all exposed to ambient conditions, they experience carbonation to different degrees. It appears that the top of the cylinder is subjected to more severe carbonation than the other parts as indicated by more pronounced characteristic peaks. This is due to different mechanisms between dry and wet carbonations [52–54]. In the "bot" part, the paste is submerged in deionized water. Due to the gradient of ion concentration, Ca^{2+}, Na^{+} and OH^{-} ions can leach away from the bottom of cylinders, which increases the pH of the leachate. Under alkaline conditions, gaseous CO_2 can hydrolyse to CO_3^{2-} ions, which then react with Ca^{2+} ions to the precipitation of $CaCO_3$ on the surface of cylinders or in the leachate [43]. In the "low" part, despite not being fully immersed in water, the paste at this location also has a relatively high saturation degree, which may follow the same wet carbonation mechanism as that in the "bot" part. However, on the "top" part of the cylinders, the paste is situated at a relatively high position and exposed to dry air, which is vulnerable to dry carbonation [52, 55–57]. As reported in [58], calcium carbonate and carbonated hydrotalcite-like phases are the two main CO_2-bearing phases upon dry or ambient carbonation. Due to a probably higher concentration of CO_2 in the air than in the leachate and the higher diffusion coefficient of CO_2 in the dry matrix, dry carbonation appears to be more intensive than wet carbonation during the same exposure time [53]. This is supported by more evident peaks of calcite in the "top" paste. Interestingly, calcium

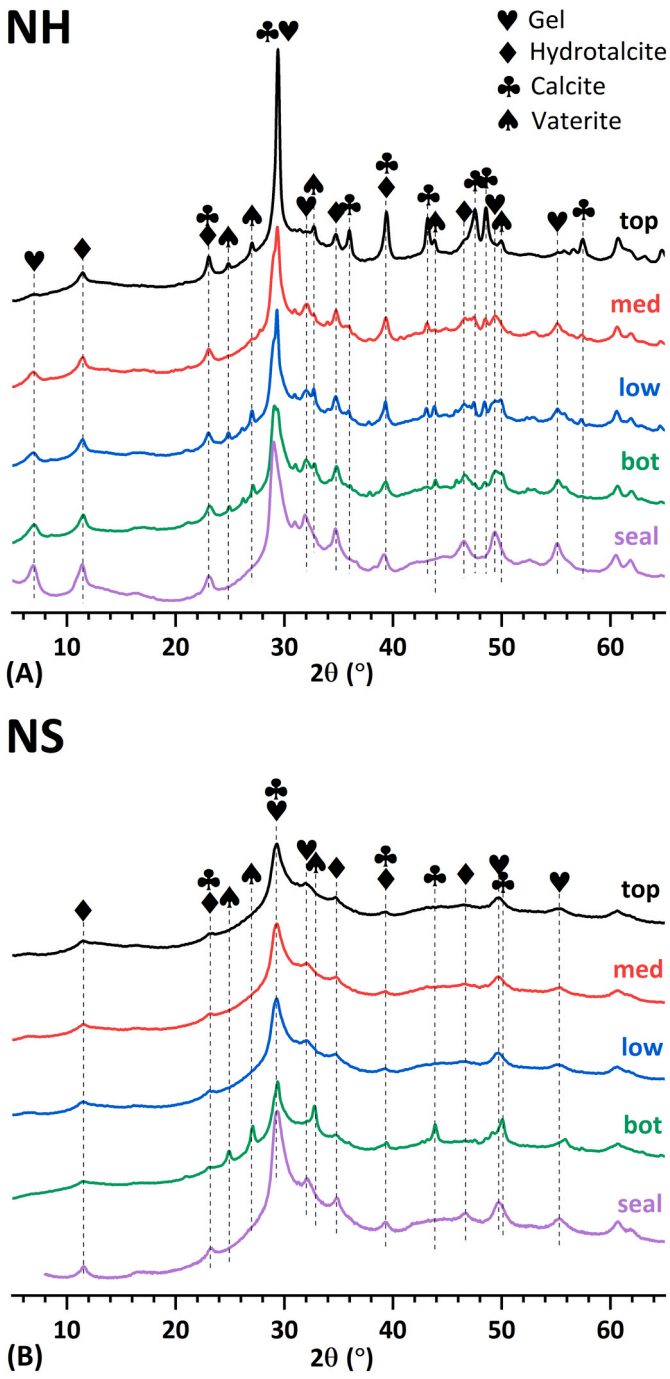

Fig. 14. XRD pattern of 7 d (A) NH and (B) NS pastes subjected to 28 d of efflorescence under ambient conditions and 28 d of sealed conditions. The labels "top", "med", "low" and "bot" represent the top, medium, low and immersed parts of the AAS cylinder under ambient conditions, respectively. The label "seal" denotes the AAS paste under sealed conditions.

carbonate is rarely detected in the paste located at the "med" position, at which the efflorescence product of sodium carbonate emerges (Fig. 5). This is likely due to a conducive RH for the growth of Na_2CO_3 in the "med" region and a considerably higher concentration of Na^+ ions than Ca^{2+} ions in an AAS system. Furthermore, the characteristic peaks of gels in the pastes under sealed conditions remain more evident than those under ambient conditions, and the reflection of gels of paste at the "top" is less intense than the others. These can be attributed to gel decalcification caused by wet and dry carbonation to different extents. As for hydrotalcite-like phases, no significant differences are identified among the five pastes, as the characterization peak of hydrotalcite is almost the same as that upon carbonation [59]. This indicates that hydrotalcite is stable to wet or dry carbonation.

Fig. 14B shows the XRD pattern of 7 d NS pastes subjected to 28 d of efflorescence under ambient conditions and 28 d of sealed conditions, respectively. Despite the two phases of gels and hydrotalcite being the same as identified in NH pastes, their characteristic peaks in NS pastes are less evident, indicating a more amorphous structure of reaction products in the NS system [60,61]. Different from that in NH samples, calcium carbonate is only identified in the "bot" part of the NS cylinder. On one hand, this suggests that NS pastes are less susceptible to dry carbonation, consistent with results reported in [31,62]. The primary reason is a lower content of Ca in both the pore solution and interlayer of gels [43,60], leading to reduced formation of calcium carbonate compared to NH systems. On the other hand, as shown in Fig. 5, the efflorescence products on NS cylinders initiate from the "low" position and develop to the top gradually. This observation again proves that $CaCO_3$ does not form in the region where efflorescence happens. Regarding the gel and hydrotalcite-like phases, NS pastes at different levels show limited discrepancies.

3.3.2. TGA

Fig. 15 shows the TG and DTG curves of 7 d NH and NS pastes subjected to 28 d of efflorescence under ambient conditions and 28 d of sealed conditions. According to the literature [63], weight loss below 200 °C corresponds to the release of water from gels, while hydrotalcite-like phases mainly undergo decomposition at around

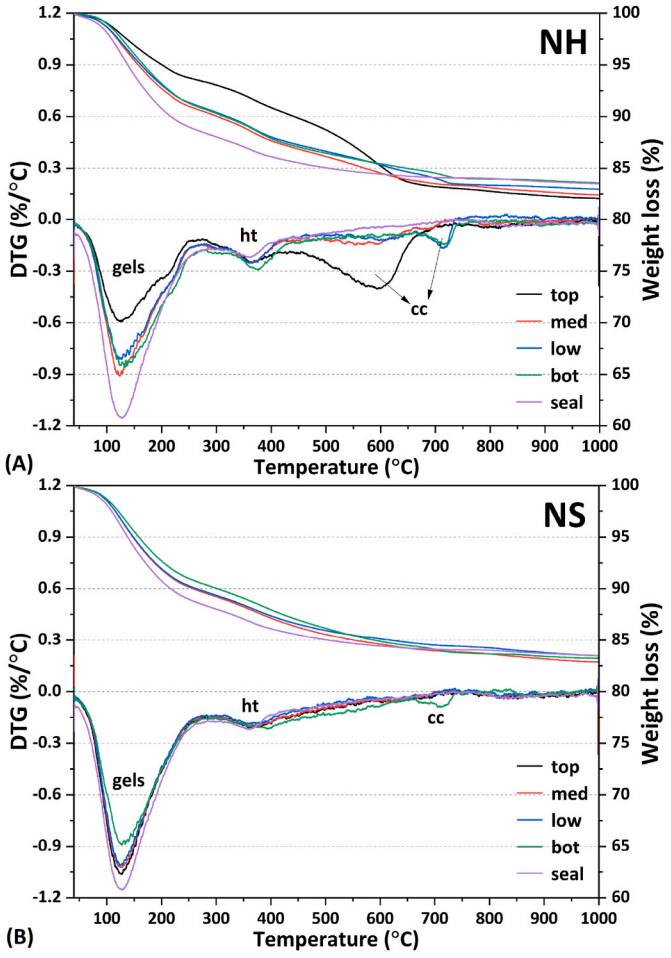

Fig. 15. TG and DTG curves of 7 d (A) NH and (B) NS pastes subjected to 28 d of efflorescence under ambient conditions and 28 d of sealed conditions. ht: hydrotalcite-like phases; cc: calcium carbonate.

200–250 and 300–400 °C [59]. Due to the different chemical structures of calcium carbonate, amorphous/poorly-crystalized $CaCO_3$, aragonite, vaterite, and calcite are decomposed at temperatures around 450–530 °C, 530–650 °C, and 650–950 °C, respectively [50,64].

Fig. 15A shows the TG and DTG curves of NH samples. The weight loss of gels and hydrotalcite-like phases (ht) is identified in the sealed sample. Besides, the peak of gels is more significant in the sealed sample than in exposed samples. This weight loss in gels is associated with both a higher content of gels and a higher content of chemically bound water in gels. The former lies in the fact that the sealed condition is conducive to the reaction of slag and the formation of gels, while the latter results from the reduction of interlayer Ca or Na in gels caused by carbonation or efflorescence, which subsequently decreases the chemically bound water of cations in the gels. In addition to the sealed condition, the cylinder under ambient conditions contains different contents and types of $CaCO_3$ at different heights. Specifically, the decomposition peak of calcium carbonate in the "top" of NH cylinders ranges from 45 to 750 °C. Combined with the above XRD results (Fig. 14A), this indicates the presence of amorphous $CaCO_3$, vaterite and calcite, which resembles that in NH pastes upon natural carbonation [31,63,65]. In the "bot" and "low" parts, the pastes undergo wet carbonation, and the decomposition temperature of calcium carbonate is much higher than that in the "top" region, indicating a more stable polymorph (calcite). The formation of different $CaCO_3$ polymorphs under dry and wet carbonation is probably dependent on the specific location of the carbonation reaction [53]. Under dry conditions, the pore structure is less saturated. The carbonation reaction can happen in both the pore solution and gel structure. The free Ca^{2+} ions in the pore solution have a relatively large space for the formation of $CaCO_3$, which contributes to the formation of calcite (Fig. 14A). However, the Ca located in the gel structure has less space, allowing only the formation of vaterite and amorphous $CaCO_3$. Under wet conditions, the water content in pores becomes higher, which leads to the leaching of interlayer Ca in gels. The leached Ca migrates to the pore solution and promotes the formation of crystalline calcium carbonate. Moreover, the content of $CaCO_3$ in the "top" part is much higher than that in the "bot" and "low" parts and no evident decomposition peak of calcium carbonate is found in "med". These observations align well with the above XRD results (Fig. 14A).

Fig. 15B shows the TG and DTG curves of NS pastes. Generally, the total weight loss of NS pastes is comparable to that of NH pastes. Two decomposition peaks corresponding to gels and hydrotalcite-like phases are observed in NS pastes. The intensity of the gel peak in the sealed paste is higher than that at other positions, similar to the TGA results of NH pastes. Additionally, $CaCO_3$ is exclusively detected in the "bot" part of cylinders, which matches well with the XRD results (Fig. 14B). Interestingly, the water-immersed part of the cylinder exhibits a lower content of gels than the other three groups. This is probably due to the leaching and carbonation of gels [5,43].

3.3.3. FTIR

Fig. 16 shows the FTIR pattern of AAS pastes subjected to 28 d of efflorescence under ambient conditions and 28 d of sealed conditions. It is observed that all the FTIR pattern is dominated by a hump around 950 cm^{-1}, which is associated with the asymmetric stretch of Si-O bonds generated by Q^2 units in gels [31]. A shoulder on the low-frequency side of this hump is located at 895 cm^{-1}, referring to the bending vibration of Si-O. Besides, the peak at around 875 cm^{-1} is assigned to the out-of-plane bending of CO_3^{2-} in calcium carbonate.

Fig. 16A shows the FTIR pattern of NH pastes. It is observed that the peak value of Q^2 units ranges from 943 cm^{-1} to 960.9 cm^{-1} in the five pastes. A higher wavenumber of the Q^2 peak indicates a higher polymerization degree of gel structure [66]. The peak value of Q^2 units in the "top" paste is much higher than that in the remaining four pastes. This is mainly due to gel decalcification caused by dry carbonation [67]. Solid-state nuclear magnetic resonance (NMR) is an advanced characterization technique that provides detailed insights into gel structure. Studies using this method have shown significant decalcification of the gel after carbonation, which in turn promotes the formation of aluminosilicate gels [29,68]. These gels are highly amorphous and are characterized by an increased presence of Q^3 and Q^4 species. To some extent, our FTIR results also support these observations, as the broader width of the main peak in the sealed sample suggests a more disordered gel structure.

Additionally, the peak values of the "med", "low" and "bot" pastes are comparable, higher than those of the paste under sealed conditions. The elevated polymerization of gel structure in "low" and "bot" can be

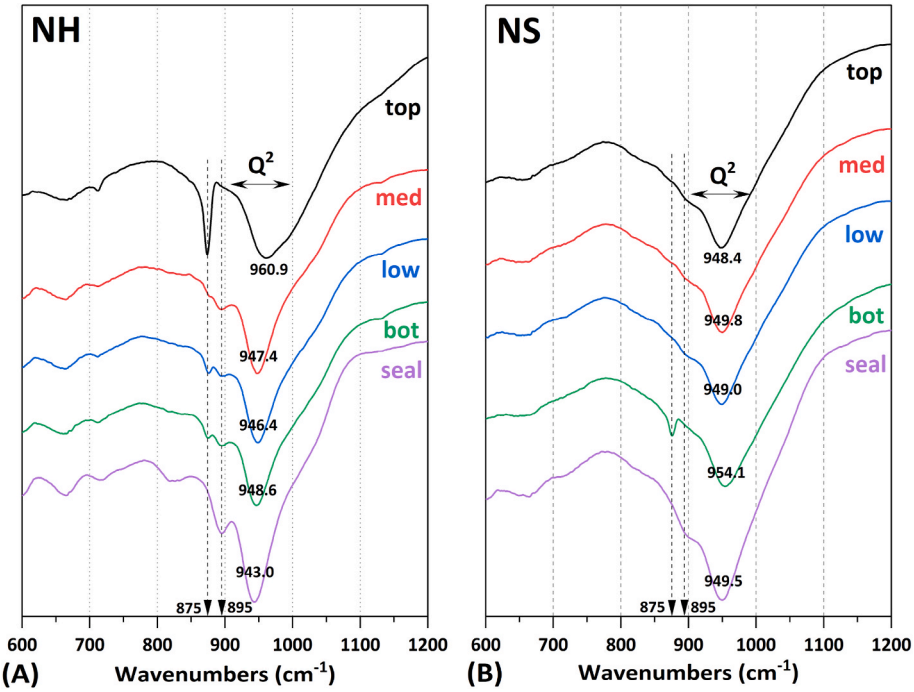

Fig. 16. FTIR pattern of 7 d (A) NH and (B) NS pastes subjected to 28 d of efflorescence under ambient conditions and 28 d of sealed conditions.

attributed to gel decalcification caused by wet carbonation. However, in the paste of "med", carbonation of pastes is rarely detected in XRD, TGA and FTIR results, thereby this phenomenon cannot be directly ascribed to the carbonation of Ca. Liu et al. [5] investigated the structural change of C-(N-)A-S-H gels induced the leaching of Na. They found that the leaching of interlayer Na prompts the movement of Ca from intralayer to interlayer, which results in the decalcification of the Ca-O sheet in silicate chains. In the "med" region of NH cylinders, efflorescence products form considerably as shown in Fig. 5. The leaching of Na in gels may occur for the formation of sodium carbonate, resulting in an increased length of gels. Moreover, the reflection of C-O units at 875 cm^{-1} is prominently present in the "top" part of the NH cylinder, as an indicator of a substantial presence of calcium carbonate. The presence of C-O units in "low" and "bot" pastes is also identified but the content is very low. These observations are all in agreement with XRD and TGA results.

Fig. 16B shows the FTIR pattern of NS cylinders. The peak value of Q^2 units ranges from 948.4 cm^{-1} to 954.1 cm^{-1} in the five NS pastes, which is generally higher than that of NH pastes, except for the "top" of NH cylinders. With equivalent alkali dosage, gels in NS pastes have a lower Ca/Si ratio than NH pastes, resulting in a higher polymerization of gels in NS pastes [43]. Besides, the peak values of "top", "med", "low" and "seal" are comparable, which are lower than that of "bot". Integrating the results of XRD, TGA and FTIR, it can be found that calcium carbonate is only identified in the "bot". Therefore, the elevated polymerization degree of gels is due to the wet carbonation of gels [53] and the leaching of Na [5]. The out-of-plane bending of C-O in calcium carbonate is also detected in the "bot" part of NS cylinders, consistent with XRD and TGA results.

Table 3
The porosity of NH and NS pastes considering the pores ranging from 7 nm to 400 μm.

	Porosity (%)		Porosity (%)
NH_top	23.7	NS_top	10.3
NH_med	24.5	NS_med	8.9
NH_low	22.4	NS_low	9.4
NH_bot	24.5	NS_bot	10.1
NH_seal	25.9	NS_seal	9.9

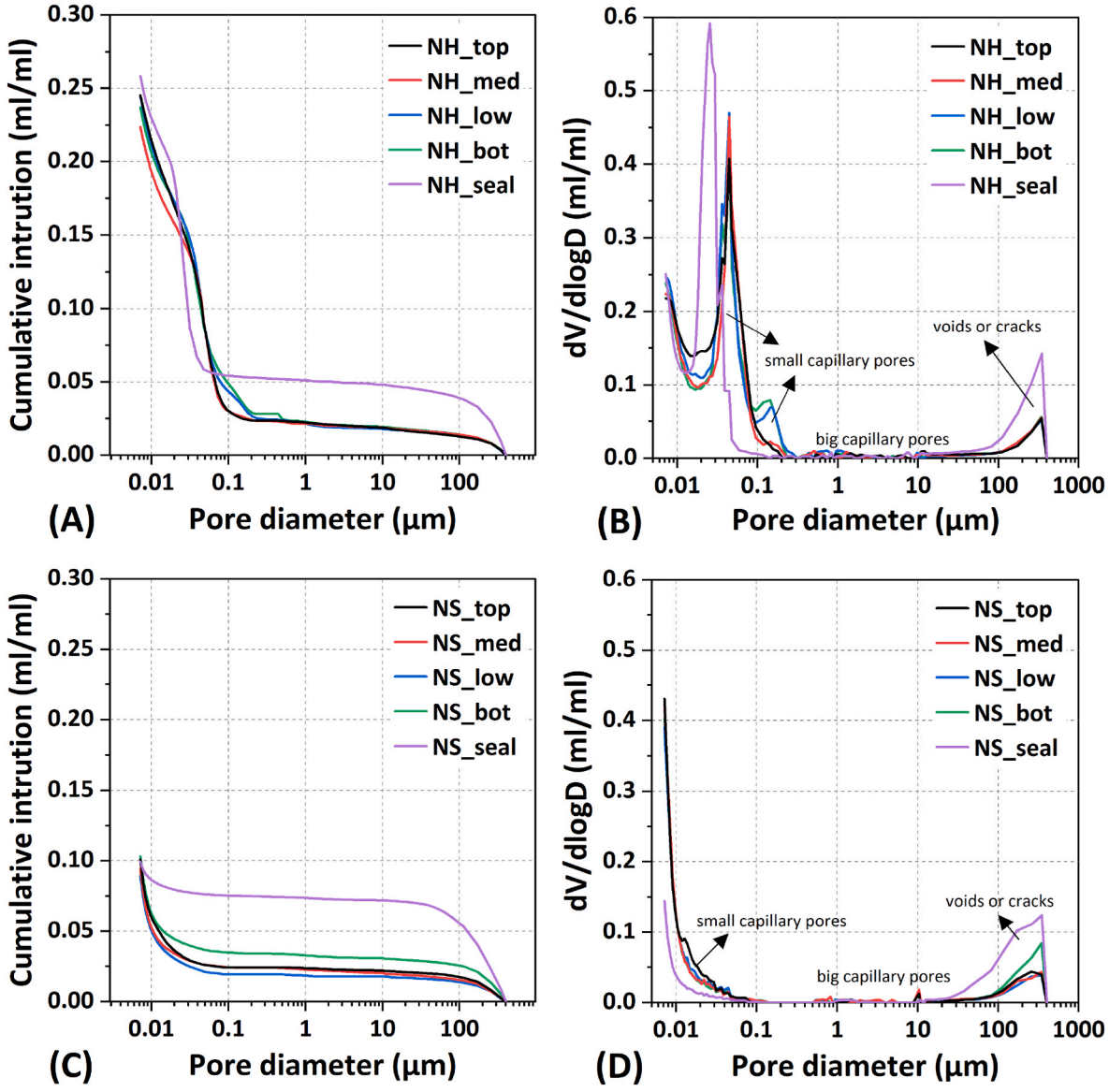

Fig. 17. Cumulative pore volume and pore size distribution of 7 d NH and NS pastes subjected to 28 d of efflorescence under ambient conditions and 28 d of sealed conditions.

3.3.4. MIP

Fig. 17 shows the cumulative pore volume and pore size distribution of 7 d NH and NS pastes subjected to 28 d of efflorescence under ambient conditions and 28 d of sealed conditions. Table 3 presents the porosity of AAS pastes, considering the pores ranging from 7 nm to 400 μm. Normally, pores in building material are broadly categorized into gel pores (0.001–0.01 μm), small capillary pores (0.01–1 μm), big capillary pores (1–100 μm) and voids or cracks (>100 μm) [69]. Generally, the porosity of NS pastes is significantly lower than that of NH pastes, due to the presence of silicates in the activator of NS systems. In terms of NH pastes, the porosity of "top", "med", "low" and "bot" are comparable, ranging from 22 % to 24 %, which is lower than that of "seal". This result is consistent with findings reported in [31,70], where the NH paste under ambient conditions shows lower porosity than under sealed conditions. This is attributed to the presence of Ca in the pore solution, which promotes the formation of calcium carbonate under ambient conditions — a volume expansion reaction that subsequently densifies the pore structure. This might be validated by Fig. 17B, in which the paste under sealed conditions shows a higher volume of large pores (100–400 μm) than that under ambient conditions. These large pores are probably due to the cracks induced by shrinkage, which is seemingly refined by the formation of calcium carbonate under ambient conditions. Additionally, the average diameter of capillary pores in sealed NH pastes is smaller than that in ambient NH pastes. This probably indicates that sealed curing contributes to a better reaction of slag and the formation of reaction products.

The total porosity of NS paste under sealed and ambient conditions is comparable (Fig. 17C and Table 3). However, the pore size distribution between them is different, as shown in Fig. 17D. Specifically, the NS paste under sealed conditions shows a high volume of large pores but a lower volume of small capillary pores and gel pores, which is also consistent with the pore size distribution of NH paste. This indicates that the refinement of voids and cracks is compromised by the coarsening of small capillary pores and gel pores. However, the pore refinement by carbonation is not that efficient in NH pastes, since there is less Ca available to be carbonated to form calcium carbonate, as presented in XRD, TGA and FTIR results. Even worse, as discussed above, the cracking of NS cylinders can be exacerbated by the formation of efflorescence products, which may further compromise the positive effect of calcium carbonate formation. Overall, 28 d of efflorescence shows limited influence on the total porosity of both NH and NS pastes but can affect their pore size distributions.

3.3.5. Compressive strength

Fig. 18 shows the compressive strength of NH and NS pastes under "ambient", "ambient_bot" and "N_2_bot" conditions. Generally, the compressive strength of NS pastes is significantly higher than that of NH pastes, corresponding to the MIP results. As shown in Fig. 18A, the compressive strengths of NH prisms exposed to three conditions all increase with time. The compressive strengths of NH prisms exposed to the "ambient_bot" condition at 7 and 28 d are slightly lower than those under ambient and "N_2_bot" conditions, which suggests that efflorescence shows barely adverse impact on the compressive strength of NH pastes. As shown in Fig. 6, the NH cylinders, after exposure to "ambient_bot" and "N_2_bot" conditions for 28 d, exhibit no visible surface cracks. These results imply that neither the uneven distribution of humidity nor the crystallization pressure induced by efflorescence leads to significant structural problems in the matrix of NH pastes.

However, efflorescence shows significantly adverse impacts on the compressive strength of NS pastes. As shown in Fig. 18B, the compressive strength of NS specimens under "ambient_bot" condition is lower than that under ambient conditions. Márlon et al. [71] investigated the compressive strength of metakaolin-based geopolymers under sealed, efflorescence, carbonation and leaching conditions. They found that the

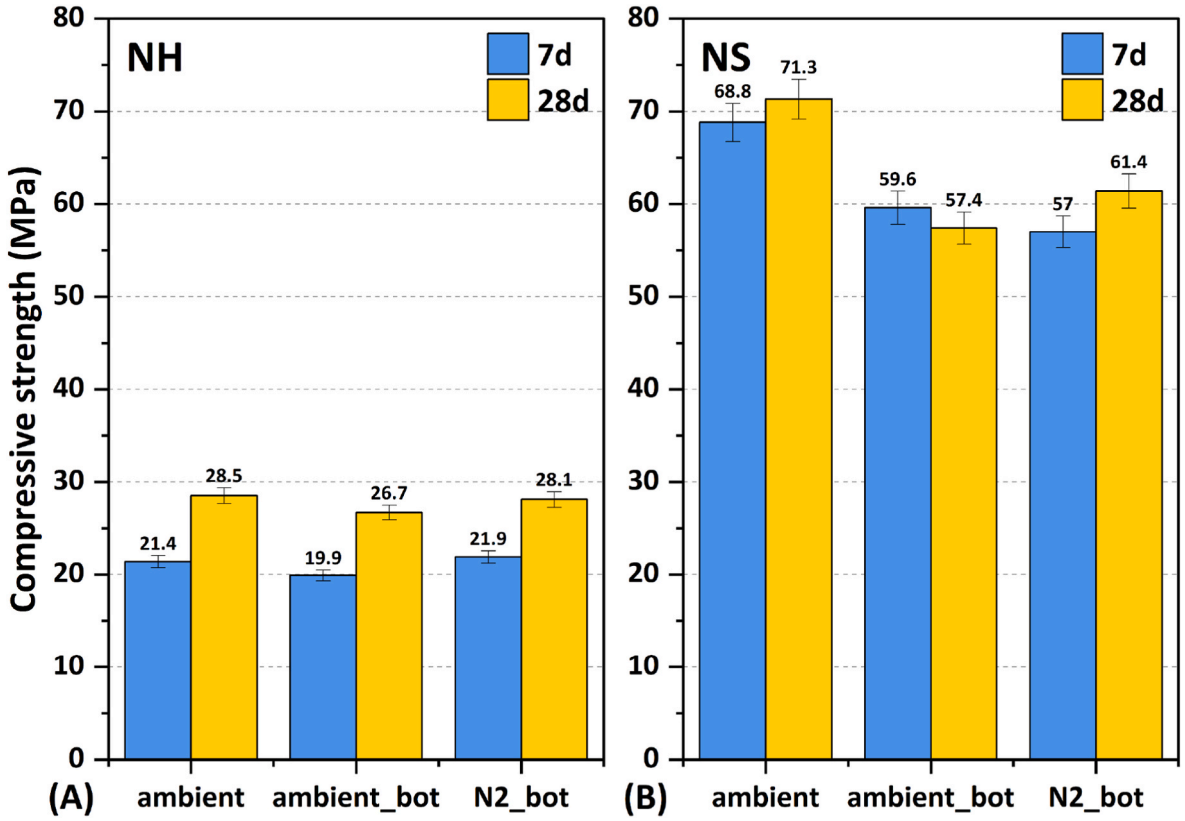

Fig. 18. Compressive strength of (A) NH and (B) NS pastes sealed for 7 d followed by exposure to ambient, "ambient_bot", and "N_2_bot" conditions for 7 and 28 d "ambient" represents a room environment with T = 20 °C and RH = 55 %. "ambient_bot" refers to the bottom of prisms in contact with water under ambient condition. "N_2_eff" denotes the bottom of prisms in contact with water under N_2 conditions.

compressive strength of samples exposed to efflorescence is lower than that of samples under natural carbonation. On one hand, Na leaching from the bottom of the samples deteriorates the microstructure (Table 3). On the other hand, the "ambient_bot" condition induces an uneven distribution of water content, which further leads to an uneven distribution of internal stress and the formation of cracks [41]. Additionally, excessive formation of efflorescence products along the cracks results in volume expansion and crack propagation. The compressive strength of NSpastes under "N_2_bot" condition can support this statement. At 7 d, the compressive strength of prisms under "N_2_bot" condition is lower than that under both "ambient" and "ambient_bot" conditions. This indicates that even without efflorescence, the semi-contacted water condition has already induced significant reductions in compressive strength. In addition, the slightly lower value of "N_2_bot" compared to "ambient_bot" at 7 d is probably because the efflorescence products formed at early ages can partially densify the cracks. Noted that the samples with efflorescence products were not ultrasonically cleaned before compressive tests. However, at 28 d, the compressive strength of NS samples exposed to the "ambient_bot" condition is lower than that under "N_2_bot" condition. This implies that prolonged formation of efflorescence products exacerbates the cracking issue. Therefore, AAS paste with a high silicate modulus is more susceptible to efflorescence in terms of compressive strength.

4. Discussion

4.1. Efflorescence process of AAS pastes

Accordingly, the efflorescence of AAS cylinders under ambient conditions is observed and the impact of efflorescence on AAS pastes is investigated. Based on these findings, the efflorescence process of NH and NS pastes can be deduced. Fig. 19 depicts a schematical representation of the process of efflorescence of AAS pastes under ambient conditions. Given the different chemical composition and pore structure between the NH and NS pastes, it is necessary to discuss them separately.

Fig. 19A demonstrates the efflorescence process of NH pastes. Generally, the paste with its bottom in contact with water can be divided into underwater and overwater parts by the waterline. In the underwater part, the paste is subjected to leaching. Due to the gradient of ion concentration, Na^+, Ca^{2+} and OH^- ions in the pore solution can leach away from the paste, which can increase the pH of the leachate. An alkaline condition facilitates the dissolution of gaseous CO_2 and contributes to the formation of CO_3^{2-} by hydrolysis. The resulting CO_3^{2-} can further react with Ca^{2+} to the precipitation of $CaCO_3$ attached to the "bot" of samples.

Once the underwater region has been entirely infiltrated, moisture continues to migrate upward. In the area nearly above the waterline ("low" sections), a water film on the surface of the sample forms. Gaseous CO_2 can dissolve into this water film and hydrolyse to CO_3^{2-}, in the meantime, Na^+ and Ca^{2+} ions can migrate to the surface from the matrix, contributing to the formation of Na_2CO_3 and $CaCO_3$. However, as a result of the high humidity at the "low" position, the efflorescence product of Na_2CO_3 crystals is soluble in this zone, hence the main CO_2-bearing phase is $CaCO_3$.

As the increase of the height of the cylinder, the RH of pastes would gradually decrease. There is an area in which sodium carbonate is more likely to form. In the case of the NH paste, the efflorescence front is located in the medium part, while that of the NS paste is located at a lower position. This is due to a more porous structure of the NH paste, contributing to an increased water sorptivity of cylinders and a higher fraction of high-humidity regions. Besides, $CaCO_3$ is barely identified at the region where efflorescence emerges, which indicates a preferential formation of Na_2CO_3 over $CaCO_3$. NH pastes after 28 d of efflorescence show limited cracks on the surface. The efflorescence products accumulate progressively around the efflorescence front. As for the "top" part, the paste at this location is relatively dry, akin to dry carbonation, where $CaCO_3$ emerges as the main CO_2-bearing product.

Fig. 19B depicts the efflorescence process of NS paste. Similar to the NH pastes, calcium carbonate is detected in the "bot" of the NS cylinder, resulting from the leaching of Ca^{2+} ions in the matrix and the solvent

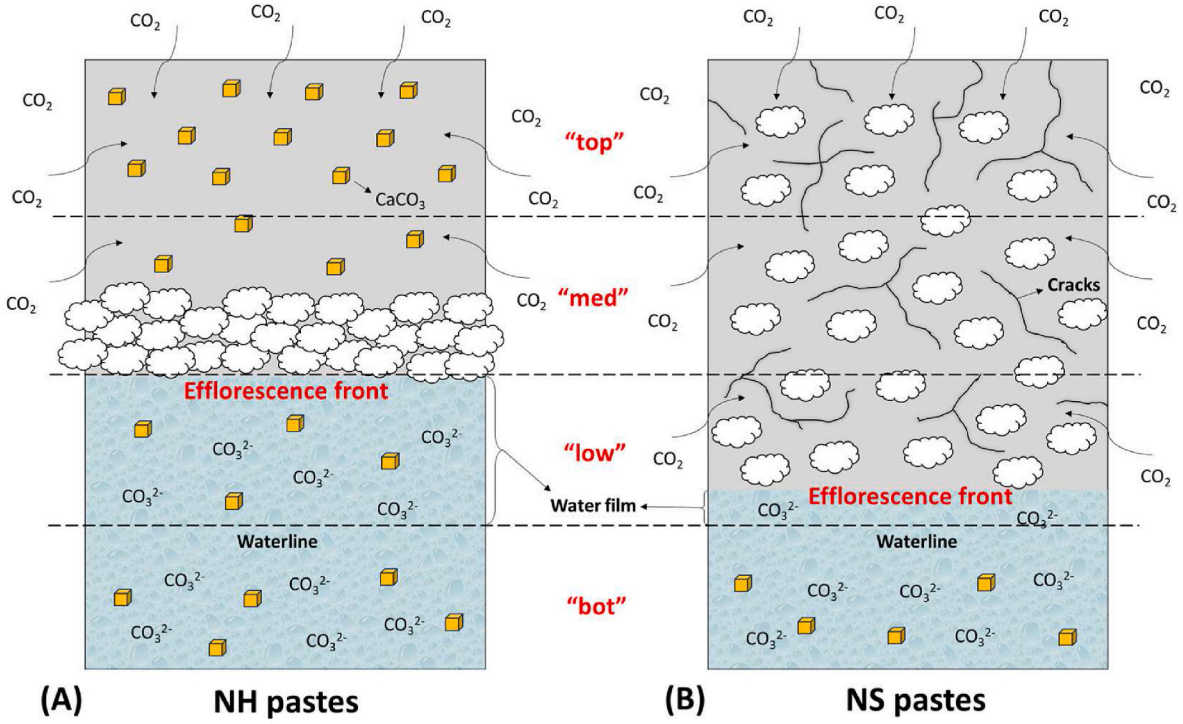

Fig. 19. Schematical representation of the process of efflorescence of (A) NH and (B) NS pastes under ambient conditions. The white cloud-like shape refers to the efflorescence products (sodium carbonate), and the golden cubic shape refers to the carbonation products (calcium carbonate). (For interpretation of the references to colour in this figure legend, the reader is referred to the Web version of this article.)

CO_3^{2-} ions from the air. Due to the lower porosity of the matrix, the efflorescence front of the NS paste is lower than that of the NH paste. However, the efflorescence product of NS pastes can develop toward a higher position than NH pastes. This phenomenon is probably attributed to the cracking of NS cylinders under such semi-contact water conditions, which can promote the transport of water and alkali ions. Additionally, the cracking problem can be exacerbated by the formation of efflorescence products. Similar to NH pastes, calcium carbonate is absent in the efflorescence regions of NS cylinders ("low", "med" and "top"). This again indicates a competition between efflorescence and carbonation.

4.2. Efflorescence mechanisms of AAS pastes

For a better understanding of the mechanisms of efflorescence of AAS pastes, it is essential to focus on the formation of efflorescence products (hydrated sodium carbonate). Fig. 20 shows the chemical reaction of efflorescence formation. It can be seen that Na^+, CO_3^{2-} and H_2O are the three main components contributing to the formation of hydrated sodium carbonate. The availability of them is influenced by alkali dosages, pore structure and environmental conditions.

4.2.1. Alkali metal ion (Na)

The Na in efflorescence products stems from the leaching of Na in AAS pastes, with most of the Na^+ ions deriving from the pore solution and a minor portion from C-(N-)A-S-H gels [27]. The overall amount of Na that can reach the water film surrounding the paste is governed by both the alkalis in the pore solution (or the initial alkali dosage in activators) and the transport of Na within the pore structure. As for the same type of AAS pastes, although a higher alkali content contributes to a denser microstructure, which can partly hinder the transport of Na^+ ions, the alkali content seems to play a more significant role than the pore structure, as observed in efflorescence experiments among "NH_3 %", "NH_5 %" and "NH_7 %". At the same alkali dosage, the compact microstructure of NS pastes can impede efflorescence during early ages but fails to prevent its occurrence at later ages. A dense matrix leads to high pore pressure and significant cracking problems. The permeability of NS pastes increases caused by surface cracks, which promotes the transport of Na and thus the formation of efflorescence products at later ages. This highlights the importance of pore structure in influencing the efflorescence.

4.2.2. CO_2

The concentration of CO_2 remains constant in the air at around 0.04 % by volume, while that in a liquid is not fixed. Therefore, it is imperative to understand the dissolution behaviour of CO_2 in an aqueous condition. Typically, CO_2 can first react with water to form H_2CO_3 molecules slowly, as shown in Eq. (1) [72,73]. Under weak alkali conditions with a pH < 8, these H_2CO_3 molecules react with OH^- to yield bicarbonate ions (HCO_3^-), as expressed in Eq. (2) [74]. In cases where the alkali solution is fairly concentrated with a pH > 10, CO_2 can directly react with OH^- to form HCO_3^-, which further reacts with OH^- to form CO_3^{2-}, as shown in Eq. (3). If the alkali is depleted or the atmospheric CO_2 is in high concentration, the CO_3^{2-} can react with CO_2 once again, forming HCO_3^-, leading to the decrease of pH of the host solution (Eq. (4)) [28,72].

$$CO_2(aq) + H_2O(l) \rightarrow H_2CO_3(aq) \quad \text{Eq. 1}$$

$$H_2CO_3(aq) + OH^-(aq) \rightarrow HCO_3^-(aq) + H_2O(l) \quad \text{Eq. 2}$$

$$HCO_3^-(aq) + OH^-(aq) \rightarrow CO_3^{2-}(aq) + H_2O(l) \quad \text{Eq. 3}$$

$$CO_3^{2-}(aq) + H_2O(l) + CO_2(aq) \rightarrow 2HCO_3^-(aq) \quad \text{Eq. 4}$$

According to these equations, the type and amount of hydrolyzed CO_2 species are closely dependent on the pH of the host solution. In the case of efflorescence, the host solution refers to the water film above the waterline (Fig. 19). The pH of this water film is influenced by the leaching of OH^- from the AAS matrix. Given the high alkalinity of the pore solution in AAS materials (typically above 14) [43,75], the pH of the water film can easily exceed 13. Under such conditions, CO_3^{2-} ions dominate in the host solution, as indicated by Eq. (3), promoting the formation of hydrated sodium carbonate. This is supported by the XRD results of the efflorescence products under ambient conditions (Fig. 13). However, the concentration of CO_2 can impact the phase assemblage of efflorescence products. Fig. A1 shows the XRD pattern of efflorescence products from AAS pastes exposed to 0.2 % CO_2 conditions. In this case, trona ($Na_3H(CO_3)_2{\cdot}2H_2O$), a combination of $NaHCO_3$ and Na_2CO_3, emerges as the primary efflorescence product on NH pastes. This suggests that elevated CO_2 concentrations result in the regeneration of HCO_3^- ions in the water film (Eq. (4)). Therefore, considering the complexity of the pH of the water film and the anion in efflorescence products, it is more accurate to quantify efflorescence by determining the amount of Na.

4.2.3. Water (or RH)

Water serves as the media of chemical reactions, significantly impacting the visibility and chemical-bound water of efflorescence products. A relatively low RH is favourable for both the rate and severity of efflorescence formation of AAS pastes when the bottom of the samples is in contact with water, as observed in the efflorescence tests among "NH_40 %", "NH_60 %" and "NH_80 %". Conversely, a high RH results in the dissolution of efflorescence products and a reduction in visible efflorescence. Additionally, water transport can affect the chemical-bound water of efflorescence products. Sodium carbonate on the NH paste shows a higher content of chemically bound water compared to the NS one. This is related to the porous pore structure of the NH pastes, which provides the crystallization of sodium carbonate with more water.

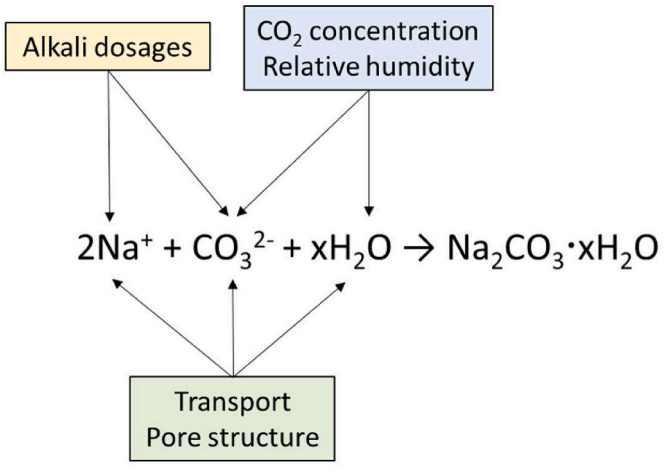

Fig. 20. Formation mechanisms and influential factors of efflorescence products of AAS pastes.

5. Conclusions

In this study, the effects of alkali dosages, activator types, exposure atmospheres, and relative humidities on the efflorescence of AAS pastes are observed. The leaching tests of pastes in different sizes are performed. The influence of efflorescence on phase assemblage, gel structure, pore structure and compressive strength of AAS pastes are examined as well. Based on the above results, the process and mechanism of efflorescence of AAS pastes have been clarified. Some conclusions are summarized as follows.

1. At the same alkali dosage, NH pastes have more porous microstructures and show higher efflorescence rates than NS pastes. The NH paste with a higher alkali dosage shows more severe efflorescence. The NH paste subjected to a lower RH environment shows a more rapid and significant efflorescence. The NS paste suffers from cracking problems when the bottom is in contact with water under both N_2 and ambient conditions. Furthermore, the formation of efflorescence products exacerbates this cracking problem.
2. The efflorescence front of AAS pastes is associated with the pore structure. The paste with a higher porosity shows a higher efflorescence front. The efflorescence products of NH pastes accumulate near the efflorescence front, while those of NS pastes develop on the top. This is attributed to the cracking of NS cylinders, which promotes the transport of water and alkali ions and the formation of efflorescence products.
3. It is feasible to quantitatively determine the efflorescence of AAS pastes by calculating the amount of Na in efflorescence products. The quantitative results are not only consistent with visual observations but also correlate with the leaching result of AAS pastes. However, it should be noted that the leaching results of NS cylinders fail to establish a good relationship with efflorescence due to the cracking problem under immersed conditions. Therefore, to predict the efflorescence of AAS pastes, it is recommended to evaluate the leaching test based on piece samples.
4. The efflorescence products of NH and NS pastes are both dominated by sodium carbonate, with different chemical-bound water contents. Sodium carbonate in NH pastes has a higher content of chemical-bound water. This is due to a more porous structure of NH pastes, which allows for a greater supply of water from the bottom of cylinders for the formation of sodium carbonate. A higher CO_2 concentration results in the efflorescence product shifting from sodium carbonate to sodium bicarbonate.
5. The water-immersed part of the pastes is subjected to wet carbonation, while the overwater part is subjected to both efflorescence and dry carbonation. However, these two chemical processes cannot happen simultaneously. Calcium carbonate is rarely found in the region where sodium carbonate forms. Additionally, 28 d of efflorescence shows limited influence on the total porosity but can affect the pore size distribution of AAS pastes.
6. The impact of efflorescence on the compressive strength of NH pastes is minimal but is significant for NS pastes. The compressive strength of NS specimens after 28 d of efflorescence is lower than that under ambient conditions, which is even lower than that after 7 d of efflorescence. The reduction is probably owing to cracking by heterogeneous internal stress coupled with the expansion caused by the formation of efflorescence products. Efflorescence is detrimental to the development of long-term mechanical properties of AAS materials. Further work is necessary to comprehensively understand the impact of efflorescence on the durability of materials.

CRediT authorship contribution statement

Chen Liu: Writing – original draft, Methodology, Investigation, Funding acquisition, Conceptualization. **Zhenming Li:** Writing – review & editing, Supervision. **Guang Ye:** Writing – review & editing, Supervision, Project administration.

Declaration of competing interest

The authors declare that they have no known competing financial interests or personal relationships that could have appeared to influence the work reported in this paper.

Acknowledgement

Chen Liu would like to acknowledge the funding supported by the China Scholarship Council (CSC) under grant No. 201906950102. Zhenming Li would like to acknowledge the Guangdong Provincial Key Laboratory of Intelligent and Resilient Structures for Civil Engineering (2023B1212010004).

Appendix

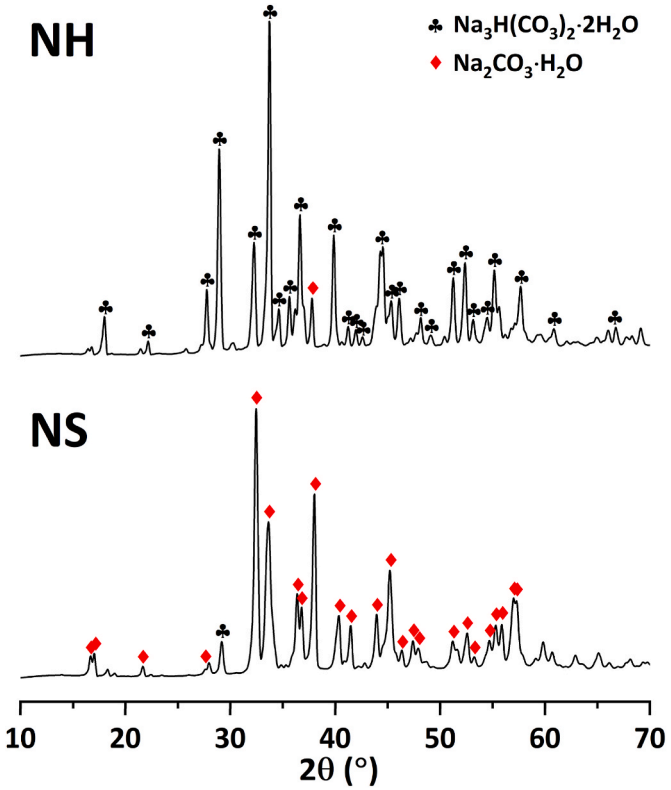

Fig. A1. XRD patterns of efflorescence products on NH and NS cylinders under 0.2 % CO_2 condition.

Fig. A1 shows the phase assemblage of efflorescence products on NH and NS cylinders under 0.2 % CO_2 condition. In the NH system, the main phase is Trona ($Na_3H(CO_3)_2·2H_2O$), considered a combination of $NaHCO_3$ and Na_2CO_3. Conversely, the efflorescence product of the NS system is dominated by Na_2CO_3. Under ambient conditions, the primary phase of the efflorescence product of AAS pastes is $Na_2CO_3·xH_2O$ (Fig. 13). Under a high CO_2 concentration condition, a conversion from Na_2CO_3 to $NaHCO_3$ occurs on NH cylinders. However, little $NaHCO_3$ is identified on the NS cylinders, possibly due to inadequate water supply from the bottom hindering the conversion to $NaHCO_3$.

Data availability

Data will be made available on request.

References

[1] P. Russell, Efflorescence and the Discoloration of Concrete, CRC Press, 1983.
[2] H. Brocken, T.G. Nijland, White efflorescence on brick masonry and concrete masonry blocks, with special emphasis on sulfate efflorescence on concrete blocks, Construct. Build. Mater. 18 (2004) 315–323, https://doi.org/10.1016/j.conbuildmat.2004.02.004.
[3] C. Dow, F.P. Glasser, Calcium carbonate efflorescence on Portland cement and building materials, Cement Concr. Res. 33 (2003) 147–154, https://doi.org/10.1016/S0008-8846(02)00937-7.
[4] A. Allahverdi, E. Najafi Kani, K.M.A. Hossain, M. Lachemi, Methods to control efflorescence in alkali-activated cement-based materials, Handb. Alkali-Activated Cem. Mortars Concr. (2015) 463–483, https://doi.org/10.1533/9781782422884.3.463.
[5] C. Liu, Z. Li, S. Nie, S. Skibsted, G. Ye, Structural evolution of calcium sodium aluminosilicate hydrate (C-(N-)A-S-H) gels induced by water exposure: the impact of Na leaching, Cement Concr. Res. 178 (2024), https://doi.org/10.1016/j.cemconres.2024.107432.
[6] Z. Zhang, H. Wang, J.L. Provis, A. Reid, Efflorescence : a critical challenge for geopolymer applications, Concr. Inst. Aust. Bienn. Natl. Conf. (2013).
[7] S. Delair, R. Guyonnet, A. Govin, B. Guilhot, Study of efflorescence forming process on cementitious materials//Etude du processus de formation des efflorescences sur des matériaux cimentaires, in: 5th Int. Conf. Concr. Under Sev. Cond. Environ. Loading, Laboratoire Central des Ponts et Chaussées, 2007, pp. 633–640.
[8] E. Najafi Kani, A. Allahverdi, J.L. Provis, Efflorescence control in geopolymer binders based on natural pozzolan, Cem. Concr. Compos. 34 (2012) 25–33, https://doi.org/10.1016/j.cemconcomp.2011.07.007.
[9] Z. Zhang, J.L. Provis, A. Reid, H. Wang, Fly ash-based geopolymers: the relationship between composition, pore structure and efflorescence, Cement Concr. Res. 64 (2014) 30–41, https://doi.org/10.1016/j.cemconres.2014.06.004.
[10] Z. Zhang, J.L. Provis, X. Ma, A. Reid, H. Wang, Efflorescence and subflorescence induced microstructural and mechanical evolution in fly ash-based geopolymers, Cem. Concr. Compos. 92 (2018) 165–177, https://doi.org/10.1016/j.cemconcomp.2018.06.010.
[11] M.A. Longhi, Z. Zhang, B. Walkley, E.D. Rodríguez, A.P. Kirchheim, Strategies for control and mitigation of efflorescence in metakaolin-based geopolymers, Cement Concr. Res. 144 (2021), https://doi.org/10.1016/j.cemconres.2021.106431.
[12] J. Wang, T. Zhou, D. Xu, Z. Zhou, P. Du, N. Xie, X. Cheng, Y. Liu, Effect of nano-silica on the efflorescence of waste based alkali-activated inorganic binder, Construct. Build. Mater. 167 (2018) 381–390, https://doi.org/10.1016/j.conbuildmat.2018.02.006.
[13] K. Sun, X. Peng, S. Wang, L. Zeng, P. Ran, G. Ji, Effect of nano-SiO2 on the efflorescence of an alkali-activated metakaolin mortar, Construct. Build. Mater. 253 (2020) 118952, https://doi.org/10.1016/j.conbuildmat.2020.118952.
[14] J.B. Wang, F.S. Li, Z.H. Zhou, P. Du, D. Xu, N. Xie, X. Cheng, Y. Liu, Effect of zeolite on waste based alkali-activated inorganic binder efflorescence, Construct. Build. Mater. 158 (2018) 683–690, https://doi.org/10.1016/j.conbuildmat.2017.10.065.
[15] X. Xue, Y.L. Liu, J.G. Dai, C.S. Poon, W.D. Zhang, P. Zhang, Inhibiting efflorescence formation on fly ash–based geopolymer via silane surface modification, Cem. Concr. Compos. 94 (2018) 43–52, https://doi.org/10.1016/j.cemconcomp.2018.08.013.
[16] D. Tang, C. Yang, X. Li, X. Zhu, K. Yang, L. Yu, Mitigation of efflorescence of alkali-activated slag mortars by incorporating calcium hydroxide, Construct. Build. Mater. 298 (2021) 123873, https://doi.org/10.1016/j.conbuildmat.2021.123873.
[17] P. Chindaprasirt, P. Jitsangiam, U. Rattanasak, Hydrophobicity and efflorescence of lightweight fly ash geopolymer incorporated with calcium stearate, J. Clean. Prod. 364 (2022) 132449, https://doi.org/10.1016/j.jclepro.2022.132449.
[18] H. Maghsoodloorad, A. Allahverdi, Efflorescence formation and control in alkali-activated phosphorus slag cement, Int. J. Civ. Eng. 14 (2016) 425–438, https://doi.org/10.1007/s40999-016-0027-0.
[19] Tao Liu, Yuxuan Chen, Bo Yuan, Weitan Zhuang, H.J.H. Brouwers, Qingliang Yu, Sodium aluminate activated waste glass: reduced efflorescence behavior by C(N)–A–S–H transformation, Cement Concr. Res. 181 (2024) 107527, https://doi.org/10.1016/j.cemconres.2024.107527.

[20] T.L. Weng, W.T. Lin, A. Cheng, Effect of metakaolin on strength and efflorescence quantity of cement-based composites, Sci. World J. 2013 (2013), https://doi.org/10.1155/2013/606524.

[21] S.P. Kang, S.J. Kwon, Effects of red mud and Alkali-Activated Slag Cement on efflorescence in cement mortar, Construct. Build. Mater. 133 (2017) 459–467, https://doi.org/10.1016/j.conbuildmat.2016.12.123.

[22] B. Wu, X. Ma, H. Deng, Y. Li, Y. Xiang, Y. Zhu, An efficient approach for mitigation of efflorescence in fly ash-based geopolymer mortars under high-low humidity cycles, Construct. Build. Mater. 317 (2022), https://doi.org/10.1016/j.conbuildmat.2021.126159.

[23] B. Wu, L. Li, H. Deng, Z. Zheng, Y. Xiang, Y. Li, X. Ma, Characteristics and mechanism of efflorescence in fly ash-based geopolymer mortars under quasi-natural condition, J. Build. Eng. 55 (2022), https://doi.org/10.1016/j.jobe.2022.104708.

[24] Y. Wang, X. Liu, W. Zhang, Z. Li, Y. Zhang, Y. Li, Y. Ren, Effects of Si/Al ratio on the efflorescence and properties of fly ash based geopolymer, J. Clean. Prod. 244 (2020) 118852, https://doi.org/10.1016/j.jclepro.2019.118852.

[25] M.A. Longhi, E.D. Rodríguez, B. Walkley, Z. Zhang, A.P. Kirchheim, Metakaolin-based geopolymers: relation between formulation, physicochemical properties and efflorescence formation, Composites, Part B 182 (2020), https://doi.org/10.1016/j.compositesb.2019.107671.

[26] X. Yao, T. Yang, Z. Zhang, Fly ash-based geopolymers: effect of slag addition on efflorescence, J. Wuhan Univ. Technol.-Materials Sci. Ed. 31 (2016) 689–694, https://doi.org/10.1007/s11595-016-1430-8.

[27] R. Jia, Q. Wang, T. Luo, Deterioration and mitigation of efflorescence of alkali-activated phosphorus slag, Construct. Build. Mater. 407 (2023) 133500, https://doi.org/10.1016/j.conbuildmat.2023.133500.

[28] S.A. Bernal, J.L. Provis, D.G. Brice, A. Kilcullen, P. Duxson, J.S.J. Van Deventer, Accelerated carbonation testing of alkali-activated binders significantly underestimates service life: the role of pore solution chemistry, Cement Concr. Res. 42 (2012) 1317–1326, https://doi.org/10.1016/j.cemconres.2012.07.002.

[29] S.A. Bernal, J.L. Provis, B. Walkley, R. San Nicolas, J.D. Gehman, D.G. Brice, A. R. Kilcullen, P. Duxson, J.S.J. Van Deventer, Gel nanostructure in alkali-activated binders based on slag and fly ash, and effects of accelerated carbonation, Cement Concr. Res. 53 (2013) 127–144, https://doi.org/10.1016/j.cemconres.2013.06.007.

[30] S.A. Bernal, R.M. de Gutierrez, J.L. Provis, V. Rose, Effect of silicate modulus and metakaolin incorporation on the carbonation of alkali silicate-activated slags, Cement Concr. Res. 40 (2010) 898–907, https://doi.org/10.1016/j.cemconres.2010.02.003.

[31] Z. Shi, C. Shi, S. Wan, N. Li, Z. Zhang, Effect of alkali dosage and silicate modulus on carbonation of alkali-activated slag mortars, Cement Concr. Res. 113 (2018) 55–64, https://doi.org/10.1016/j.cemconres.2018.07.005.

[32] J. Zhang, C. Shi, Z. Zhang, Effect of Na2O concentration and water/binder ratio on carbonation of alkali-activated slag/fly ash cements, Construct. Build. Mater. 269 (2021) 121258, https://doi.org/10.1016/j.conbuildmat.2020.121258.

[33] R. Snellings, J. Chwast, Ö. Cizer, N. De Belie, Y. Dhandapani, P. Durdzinski, J. Elsen, J. Haufe, D. Hooton, C. Patapy, M. Santhanam, K. Scrivener, D. Snoeck, L. Steger, S. Tongbo, A. Vollpracht, F. Winnefeld, B. Lothenbach, RILEM TC-238 SCM recommendation on hydration stoppage by solvent exchange for the study of hydrate assemblages, Mater. Struct. Constr. 51 (2018), https://doi.org/10.1617/s11527-018-1298-5.

[34] European committee for standardization, NEN-EN 196-1. Methods of Testing Cement - Part 1: Determination of Strength, 2016 n.d.

[35] L. Srinivasamurthy, V.S. Chevali, Z. Zhang, A. Longhi, T.W. Loh, H. Wang, Mechanical property and microstructure development in alkali activated fly ash slag blends due to efflorescence, Construct. Build. Mater. 332 (2022), https://doi.org/10.1016/j.conbuildmat.2022.127273.

[36] M. Chi, Effects of dosage of alkali-activated solution and curing conditions on the properties and durability of alkali-activated slag concrete, Construct. Build. Mater. 35 (2012) 240–245, https://doi.org/10.1016/j.conbuildmat.2012.04.005.

[37] S. Aydin, B. Baradan, Effect of activator type and content on properties of alkali-activated slag mortars, Composites, Part B 57 (2014) 166–172, https://doi.org/10.1016/j.compositesb.2013.10.001.

[38] M. Chaouche, X.X. Gao, M. Cyr, M. Cotte, L. Frouin, On the origin of the blue/green color of blast-furnace slag-based materials: sulfur K-edge XANES investigation, J. Am. Ceram. Soc. 100 (2017) 1707–1716, https://doi.org/10.1111/jace.14670.

[39] H. Ye, A. Radlińska, Shrinkage mechanisms of alkali-activated slag, Cement Concr. Res. 88 (2016) 126–135, https://doi.org/10.1016/j.cemconres.2016.07.001.

[40] C. Duran Atiş, C. Bilim, Ö. Çelik, O. Karahan, Influence of activator on the strength and drying shrinkage of alkali-activated slag mortar, Construct. Build. Mater. 23 (2009) 548–555, https://doi.org/10.1016/j.conbuildmat.2007.10.011.

[41] C. Liu, W. Haoming, L. Zhenming, S. Hu, Y. Guang, Effect of curing condition on mechanical properties and durability of alkali-activated slag mortar, Construct. Build. Mater. 439 (2024) 137376, https://doi.org/10.1016/j.conbuildmat.2024.137376.

[42] F. De'nan, M.A. Megat Johari, S.C. Anak Nyandau, N.S. Hashim, The influence of palm oil fuel ash and metakaolin on the strength of concrete and crack resistance of reinforced concrete beam: a review, World J. Eng. 20 (2023) 989–1000, https://doi.org/10.1108/WJE-01-2022-0010.

[43] C. Liu, X. Liang, Y. Chen, Z. Li, G. Ye, Degradation of alkali-activated slag subject to water immersion, Cem. Concr. Compos. 142 (2022), https://doi.org/10.1016/j.cemconcomp.2023.105157.

[44] M.H. Hubler, J.J. Thomas, H.M. Jennings, Influence of nucleation seeding on the hydration kinetics and compressive strength of alkali activated slag paste, Cement Concr. Res. 41 (2011) 842–846, https://doi.org/10.1016/j.cemconres.2011.04.002.

[45] K. Hyeok-Jung, S.P. Kang, G.C. Choe, Effect of red mud content on strength and efflorescence in pavement using alkali-activated slag cement, Int. J. Concr. Struct. Mater. 12 (2018), https://doi.org/10.1186/s40069-018-0258-3.

[46] A. Saludung, T. Azeyanagi, Y. Ogawa, K. Kawai, Effect of silica fume on efflorescence formation and alkali leaching of alkali-activated slag, J. Clean. Prod. 315 (2021) 128210, https://doi.org/10.1016/j.jclepro.2021.128210.

[47] H. Haynes, R. O'Neill, M. Neff, P. Kumar Mehta, Salt weathering of concrete by sodium carbonate and sodium chloride, ACI Mater. J. 107 (2010) 258–266, https://doi.org/10.14359/51663754.

[48] S.D. Wang, X.C. Pu, K.L. Scrivener, P.L. Pratt, Alkali-activated slag cement and concrete: a review of properties and problems, Adv. Cement Res. 7 (1995) 93–102, https://doi.org/10.1680/adcr.1995.7.27.93.

[49] I.G. Richardson, A.R. Brough, G.W. Groves, C.M. Dobson, The characterization of hardened alkali-activated blast-furnace slag pastes and the nature of the calcium silicate hydrate (C-S-H) phase, Cement Concr. Res. 24 (1994) 813–829, https://doi.org/10.1016/0008-8846(94)90002-7.

[50] G. Villain, M. Thiery, G. Platret, Measurement methods of carbonation profiles in concrete: thermogravimetry, chemical analysis and gammadensimetry, Cement Concr. Res. 37 (2007) 1182–1192, https://doi.org/10.1016/j.cemconres.2007.04.015.

[51] S.A. Bernal, J.L. Provis, R. Mejía de Gutiérrez, J.S.J. van Deventer, Accelerated carbonation testing of alkali-activated slag/metakaolin blended concretes: effect of exposure conditions, Mater. Struct. Constr. 48 (2014) 653–669, https://doi.org/10.1617/s11527-014-0289-4.

[52] M. Palacios, F. Puertas, Effect of carbonation on alkali-activated slag paste, J. Am. Ceram. Soc. 89 (2006) 3211–3221.

[53] C. Liu, Y. Zhang, M. Liang, Z. Li, G. Ye, Underwater carbonation of alkali-activated slag pastes, Construct. Build. Mater. 445 (2024) 137967, https://doi.org/10.1016/j.conbuildmat.2024.137967.

[54] P. Gaikwad, S. Sathe, Effect of fly ash on compressive strength, carbonation and corrosion resistance of reinforced concrete: a systematic review, World J. Eng. (2023), https://doi.org/10.1108/WJE-07-2023-0240.

[55] T. Bakharev, J.G. Sanjayan, Y.B. Cheng, Resistance of alkali-activated slag concrete to carbonation, Cement Concr. Res. 31 (2001) 1277–1283, https://doi.org/10.1016/S0008-8846(01)00574-9.

[56] F. Puertas, M. Palacios, T. Vázquez, Carbonation process of alkali-activated slag mortars, J. Mater. Sci. 41 (2006) 3071–3082, https://doi.org/10.1007/s10853-005-1821-2.

[57] A. Boucedra, M. Bederina, Effect of plastic aggregates addition on accelerated carbonation of sand concrete, World J. Eng. 20 (2023) 722–731, https://doi.org/10.1108/WJE-10-2021-0606.

[58] S.A. Bernal, R. San Nicolas, R.J. Myers, R. Mejía De Gutiérrez, F. Puertas, J.S.J. Van Deventer, J.L. Provis, MgO content of slag controls phase evolution and structural changes induced by accelerated carbonation in alkali-activated binders, Cement Concr. Res. 57 (2014) 33–43, https://doi.org/10.1016/j.cemconres.2013.12.003.

[59] E. Bernard, W.J. Zucha, B. Lothenbach, U. Mäder, Stability of hydrotalcite (Mg-Al layered double hydroxide) in presence of different anions, Cement Concr. Res. 152 (2022), https://doi.org/10.1016/j.cemconres.2021.106674.

[60] M. Ben Haha, G. Le Saout, F. Winnefeld, B. Lothenbach, Influence of activator type on hydration kinetics, hydrate assemblage and microstructural development of alkali activated blast-furnace slags, Cement Concr. Res. 41 (2011) 301–310, https://doi.org/10.1016/j.cemconres.2010.11.016.

[61] S.-D. Wang, K.L. Scrivener, Hydration products of alkali activated slag cement, Cement Concr. Res. 25 (1995) 561–571, https://doi.org/10.1016/0008-8846(95)00045-E.

[62] N. Li, N. Farzadnia, C. Shi, Microstructural changes in alkali-activated slag mortars induced by accelerated carbonation, Cement Concr. Res. 100 (2017) 214–226, https://doi.org/10.1016/j.cemconres.2017.07.008.

[63] L. Alarcon-Ruiz, G. Platret, E. Massieu, A. Ehrlacher, The use of thermal analysis in assessing the effect of temperature on a cement paste, Cement Concr. Res. 35 (2005) 609–613, https://doi.org/10.1016/j.cemconres.2004.06.015.

[64] H. Ye, R. Cai, Z. Tian, Natural carbonation-induced phase and molecular evolution of alkali-activated slag: effect of activator composition and curing temperature, Construct. Build. Mater. 248 (2020) 118726, https://doi.org/10.1016/j.conbuildmat.2020.118726.

[65] M. Nedeljković, Carbonation mechanism of alkali-activated fly ash and slag materials in view of long-term performance predictions. https://doi.org/10.4233/uuid, 2019.

[66] F. Spectroscopy, Structure of calcium silicate hydrate (C-S-H): near-, mid-, and, Far-Infrared Spectroscopy 48 (1999) 742–748.

[67] J.J. Chen, J.J. Thomas, H.M. Jennings, Decalcification shrinkage of cement paste, Cement Concr. Res. 36 (2006) 801–809, https://doi.org/10.1016/j.cemconres.2005.11.003.

[68] T.F. Sevelsted, J. Skibsted, Carbonation of C-S-H and C-A-S-H samples studied by 13C, 27Al and 29Si MAS NMR spectroscopy, Cement Concr. Res. 71 (2015) 56–65, https://doi.org/10.1016/j.cemconres.2015.01.019.

[69] L. Cui, J.H. Cahyadi, Permeability and pore structure of OPC paste, Cement Concr. Res. 31 (2001) 277–282, https://doi.org/10.1016/S0008-8846(00)00474-9.

[70] C.H.W.Z.L.H.S.G.Y. Liu, Effect of Curing Condition on Mechanical Properties and Durability of Alkali-Activated Slag Mortar, 2020 1934472.

[71] M.A. Longhi, E.D. Rodríguez, B. Walkley, D. Eckhard, Z. Zhang, J.L. Provis, A. P. Kirchheim, Metakaolin-based geopolymers: efflorescence and its effect on microstructure and mechanical properties, Ceram. Int. 48 (2022) 2212–2229, https://doi.org/10.1016/j.ceramint.2021.09.313.

[72] D.M. Kern, The hydration of carbon dioxide, J. Chem. Educ. 37 (1960) 14.
[73] W. Stumm, J.J. Morgan, Aquatic Chemistry: Chemical Equilibria and Rates in Natural Waters, John Wiley & Sons, 2012.
[74] K. Adamczyk, M. Prémont-Schwarz, D. Pines, E. Pines, E.T.J. Nibbering, Real-time observation of carbonic acid formation in aqueous solution, Science 326 (2009) 1690–1694.
[75] Y. Zuo, M. Nedeljković, G. Ye, Pore solution composition of alkali-activated slag/fly ash pastes, Cement Concr. Res. 115 (2019) 230–250, https://doi.org/10.1016/j.cemconres.2018.10.010.